Nanoscale

Orientational Phase Behavior of Polymer-Grafted Nanocubes

Journal:	*Nanoscale*
Manuscript ID	NR-ART-06-2019-004859.R1
Article Type:	Paper
Date Submitted by the Author:	01-Aug-2019
Complete List of Authors:	Lee, Brian; Duke University, Mechanical Engineering and Materials Science Arya, Gaurav; Duke University, Mechanical Engineering and Materials Science

Orientational Phase Behavior of Polymer-Grafted Nanocubes

Brian Hyun-jong Lee and Gaurav Arya*

Department of Mechanical Engineering and Material Science

Duke University, Durham, NC 27708, USA

E-mail: gaurav.arya@duke.edu

Phone: 919-660-5435. Fax: 919-660-8963

Abstract

Surface functionalization of nanoparticles with polymer grafts was recently shown to be a viable strategy for controlling the relative orientation of shaped nanoparticles in their higher-order assemblies. In this study, we investigated *in silico* the orientational phase behavior of coplanar polymer-grafted nanocubes confined in a thin film. We first used Monte Carlo simulations to compute the two-particle interaction free-energy landscape of the nanocubes and identify their globally stable configurations. The nanocubes were found to exhibit four stable phases: those with edge-edge and face-face orientations, and those exhibiting partially overlapped slanted and parallel faces previously assumed to be metastable. Moreover, the edge-edge configuration originally thought to involve kissing edges instead displayed partly overlapping edges, where the extent of the overlap depends on the attachment positions of the grafts. We next formulated analytical scaling expressions for the free energies of the identified configurations, which were used for constructing a comprehensive phase diagram of nanocube orientation in a multidimensional parameter space comprising of the size and interaction strength of the nanocubes and the Kuhn length and surface density of the grafts. The morphology of the phase diagram was shown to arise from an interplay between polymer- and surface-mediated interactions, especially differences in their scalings with respect to nanocube size and grafting density across the four phases. The phase diagram provided insights into tuning these interactions through the various parameters of the system for achieving target configurations. Overall, this work provides a framework for predicting and engineering interparticle configurations, with possible applications in plasmonic nanocomposites where control over particle orientation is critical.

Introduction

Self-assembly of nanoparticles (NPs) offers an attractive approach for bottom-up fabrication of materials in a highly parallelized fashion over macroscopic scales. Shaped (anisotropic) NPs, in particular, have the potential to expand the horizon of material architectures achievable through assembly, beyond close-packed structures with simple symmetries formed by spherical particles.[1] Improvements in synthesis have allowed fabrication, and subsequent assembly exploration, of a diverse set of NP shapes including ellipsoids,[2,3] rods,[4] stars,[5] triangular prisms,[6] and cubes,[7] among others.[8–14] Unlike their spherical counterparts, shaped NPs offer the unique challenge of controlling not only their translational order but also rotational order during assembly.[15–18] In general, shaped NPs exhibiting attractive interactions or subjected to strong confinement tend to form close-packed arrangements via their most prominent surfaces to maximize enthalpic interactions or translational-rotational entropy, respectively. However, in many applications such as separation membranes,[19,20] solid-state electrodes,[21,22] and plasmonic composites,[23,24] a more open structure with control over the relative distance and orientation between particles is desired.

Recently, we stumbled upon a simple strategy for controlling the orientation between faceted NPs while studying polymer-grafted silver nanocubes undergoing assembly within polymer thin films.[16,17] The experiments found that, depending on the length of the polymer grafts, neighboring NPs in the assembled particle aggregates exhibited edge-edge and edge-face configurations, in addition to the face-face configuration expected of bare NPs. We proposed that the grafts introduce an orientation-dependent steric repulsion between the nanocubes that competes with van der Waals (vdW) attraction between them, which also depends on orientation, to yield these additional edge-mediated configurations. Using Monte Carlo (MC) simulations of polymers grafted on surfaces, we showed that while the closer proximity of nanocube surfaces in the face-face configuration leads to significantly stronger vdW attraction compared to the edge-edge configuration, the face-face configuration also confines the polymer chains into a much smaller volume, leading to stronger steric repulsion.

Hence, nanocubes with short grafts that are still dominated by vdW interactions assemble into the face-face configuration expected of bare nanocubes, while those with long grafts where the steric repulsion becomes more dominant form edge-edge configurations.

While this previous work demonstrated the ability to control the relative orientations of shaped NPs based on polymer grafting, several key questions remain open that we seek to address in this work. First, the experiments observed a number of nanocube configurations *in addition* to the idealized face-face and edge-edge orientations with full and no overlap between faces considered in our previous simulations. In particular, edge-face contacts as well as imperfect face-face (with partial overlap between faces) and edge-edge contacts (with overlapping edges) were observed. Whether these "intermediate" configurations represent trapped metastable states or stable states unexplored in simulations remains unknown. Second, a more in-depth analysis of the factors affecting nanocube orientations is required. Our work so far examined only the effect of graft length and graft-cube interactions. However, the overall free energy of particle assembly is expected to be governed by other parameters capable of affecting the vdW attraction or steric repulsion between the nanocubes whose interplay determines their assembly configurations. Identifying all possible stable orientational configurations of nanocubes and constructing a "phase diagram" of these configurations in the multiparameter design space would help develop approaches for controlling the assembly of nanocubes, and other types of faceted NPs, and for reconfiguring them from one orientation to another.

In this study, we addressed these open questions through an approach combining simulations and analytical modeling. In particular, we computed via MC simulations the two-particle free energy landscapes spanning *all* possible cube orientations and separation distances for parameters found to affect vdW and steric interactions between nanocubes. By analyzing the global free energy minima from these energy landscapes, we were able to identify and characterize the stable orientational phases exhibited by the nanocubes. While computing such landscapes for every parameter combination should yield the orientational

phase diagram we seek, this procedure entails prohibitive computational costs due to the large parameter space. Hence, we adopted a different route where we analyzed the contributions of vdW and steric interactions to the overall free energy of each orientational phase, and developed simple scaling relationships for these free energies as a function of system parameters. These scaling relations were then used to construct a phase diagram of nanocube orientations over an extensive parameter space. In addition to providing researchers simple "design rules" for controlling nanocube orientations, the free energy relationships also lend new physical insights into how different properties of the nanocubes and the grafts affect their configurations. Moreover, the relationships are sufficiently simple that they can be readily adapted to other kinds of faceted particles. Overall, the results obtained here advance our understanding of how polymer grafts could be used to influence the interactions and self-assembly of shaped NPs.

Computational Methods

Overview

The experimental system underpinning this work comprises of polymer-grafted nanocubes undergoing assembly within a planar polymer thin-film. The film is sufficiently thin to prevent the nanocubes from translating or rotating in the z direction normal to the film, effectively constraining their assembly to two dimensions. At the same time, the film is thick enough to fully encapsulate the NPs, including their grafts. In this work, we investigated the free energy of interactions between a pair of such film-encapsulated, coplanar NPs as a function of their relative configuration, which can be described by three geometric variables: their center-to-center distance d and their respective orientations θ_1 and θ_2 within the x–y plane (Fig. 1). The two nanocubes were treated using a coarse-grained (CG) model that accounts for vdW interactions between the nanocubes and the conformational flexibility of the grafted chains. The free energy landscape $F(d, \theta_1, \theta_2)$ was calculated as the potential

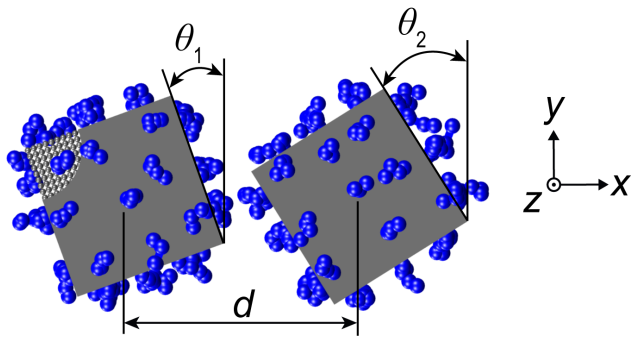

Figure 1: Schematic of simulation setup and coarse-grained model. Gray squares depict the nanocubes from top view and blue spheres represent the polymer segments. Small gray spheres shown on the left nanocube portray the underlying atomic lattice making up the nanocubes. The configuration of a two-nanocube system is fully described by distance d and orientations θ_1 and θ_2.

of mean force (PMF) defined as the restricted free energy of the system subjected to the constraints that the nanocubes are separated by a distance d and exhibit orientations θ_1 and θ_2:

$$F(d,\theta_1,\theta_2) = -k_{\mathrm{B}}T \ln \left\{ \int \cdots \int \exp\left[-\frac{U_{\mathrm{tot}}(\mathbf{r}^N, d, \theta_1, \theta_2)}{k_{\mathrm{B}}T} \right] d\mathbf{r}^N \right\}, \tag{1}$$

where the integral represents the partition function of the grafted chains integrated over their configurations $\mathbf{r}^N$ described by N Cartesian coordinates in the coordinate frames of their respective nanocubes, and $U_{\mathrm{tot}}(\mathbf{r}^N, d, \theta_1, \theta_2)$ is the total potential energy of the system. The energy landscape was computed using MC simulations, and orientational phases exhibited by the nanocubes were then identified from the global minima of such landscapes computed for a range of parameters.

CG Model

To keep the computational costs manageable, the polymer grafts and the nanocubes were treated at a CG resolution and the surrounding polymer matrix was neglected (Fig. 1). Such treatment allowed us to capture the most essential physics of this system—the interplay between shape-dependent vdW and steric interactions—with minimal number of parameters. Many previous studies have demonstrated the effectiveness of this reduced representation for

modeling polymer-grafted NPs.[25–32] The nanocubes of edge length D were constructed out of a rigid, cubic lattice of spherical atoms of size σ_{cc}. The polymer grafts were modeled as bead-chains of length L (beads), where each bead represents a polymer segment of size σ_{pol} (equal to σ_{pp}). The grafts were attached to the faces of the nanocubes in a square pattern with a spacing consistent with the grafting density Γ.

The total potential energy U_{tot} of the system included contributions from cube-cube vdW interactions U_{cc}, polymer-cube interactions U_{pc}, polymer-polymer intermolecular interactions U_{pp}, and polymer intramolecular interactions U_{intra} as given by

$$U_{\mathrm{tot}} = U_{\mathrm{cc}} + U_{\mathrm{pc}} + U_{\mathrm{pp}} + U_{\mathrm{intra}}. \tag{2}$$

U_{cc}, U_{pc}, and U_{pp} were all described using Lennard Jones (LJ) potentials

$$U_{\alpha\beta} = \sum_{i\in\alpha, j\in\beta} 4\varepsilon_{\alpha\beta}\left[\left(\frac{\sigma_{\alpha\beta}}{r_{ij}}\right)^{12} - \left(\frac{\sigma_{\alpha\beta}}{r_{ij}}\right)^{6}\right], \qquad \alpha,\beta = \text{p or c} \tag{3}$$

where the summation is carried out over all interacting atoms or beads i and j, r_{ij} is the separation distance between them, and $\sigma_{\alpha\beta}$ and $\varepsilon_{\alpha\beta}$ are the size and energy parameters of their respective interaction potentials. U_{intra} was described by harmonic bond-stretching potentials between neighboring pairs of beads and harmonic bond-bending potentials between neighboring bead triplets of the grafts:

$$U_{\mathrm{intra}} = \sum_{i\in\mathrm{bonds}} \frac{k_s}{2}(l_i - l_0)^2 + \sum_{i\in\mathrm{angles}} \frac{k_\theta}{2}(\theta_i - \theta_0)^2, \tag{4}$$

where the summation is carried out over bonds and bending angles across all the grafted chains, l_i are θ_i are the bond lengths and bending angles for the ith bead pairs and triplets; l_0 and θ_0 are their equilibrium values; and k_{s} and k_θ are spring constants. The grafts were also attached to the nanocubes via harmonic springs with the parameters k_{s} and l_0.

Model Parameters

Despite its simplicity, the above model still contains 13 parameters, all of which could potentially influence the orientational behavior of the nanocubes by affecting vdW or steric interactions. Fortunately, several of these parameters either have overlapping effects with other parameters or their magnitudes are experimentally constrained. This allowed us to narrow down the parameter space to four most relevant parameters: the nanocube size D and the interatomic interaction parameter $\varepsilon_{\mathrm{cc}}$ governing the strength of vdW attraction between the nanocubes, and the segmental excluded volume σ_{pol} and grafting density Γ of the polymer grafts expected to affect the steric repulsion between the nanocubes. Previous simulation studies on polymer-grafted spherical NPs have shown that these parameters also govern the morphology of the assembled NP aggregates.[27,28,32]

These four chosen parameters were varied within physically relevant bounds, while the remaining parameters were held fixed, also at physically reasonable values. In particular, we examined two different nanocube sizes $D = 10\sigma$ and 20σ, where σ is an arbitrary length scale taken to be the characteristic excluded volume of a polymer segment. If one considers $\sigma \sim 1$ nm, the typical Kuhn length of a polymer chain, the two NP sizes would correspond to 10 and 20 nm, respectively. The interaction strength ε_{cc} between the lattice atoms of the two nanocubes was chosen in the range 0.25–4 $k_{\mathrm{B}}T$, typical of particulate solids ranging from organic to metal crystals, such that the attractive energy at complete face-face contact was hundred- to thousand-fold larger than the thermal energy $k_{\mathrm{B}}T$. The sizes σ_{cc} of these lattice atoms, which exhibit a small experimental range, were fixed to a value of 0.4σ. For polymer grafts, we examined chains of length $L = 4$ beads and segment size σ_{pol} in the range 0.25 to 1σ attached to the nanocubes at grafting densities Γ in the range of 0.04–$0.16/\sigma^2$, corresponding to 4 to 16 chains per face of the 10σ nanocube. Under these conditions, the grafts exhibited largely mushroom conformations, even in the most densely grafted nanocubes, and produced large enough steric repulsion to affect—but not prevent—the assembly of nanocubes. The parameters $\varepsilon_{\mathrm{pp}}$ and $\varepsilon_{\mathrm{pc}}$ describing polymer-polymer and polymer-surface interactions were

Table 1: Model parameters explored in simulations.

Symbol	Description	Value
D	Edge length of a nanocube	10σ, 20σ
L	Number of beads per polymer graft	4
Γ	Grafting density	0.04–$0.16/\sigma^2$
$\varepsilon_{\mathrm{cc}}$	Energy parameter for cube-cube interactions	0.25–$4.0\ k_{\mathrm{B}}T$
$\varepsilon_{\mathrm{pc}}$	Energy parameter for polymer-cube interactions	$0.05\ k_{\mathrm{B}}T$
$\varepsilon_{\mathrm{pp}}$	Energy parameter for polymer-polymer interactions	$0.1\ k_{\mathrm{B}}T$
σ_{cc}	Size parameter for cube atoms	0.4σ
σ_{pol}	Size parameter for polymer beads	0.25–1.0σ
k_{s}	Spring constant of the harmonic stretching potential	$10\ k_{\mathrm{B}}T/\sigma$
k_θ	Bending constant of the harmonic bending potential	$0.1\ k_{\mathrm{B}}T/\mathrm{rad}^2$
l_0	Equilibrium bond length between adjacent graft beads	$1\sigma_{\mathrm{pol}}$
θ_0	Equilibrium bending angle between adjacent bonds	180°

both set to a small value of $0.1\ k_{\mathrm{B}}T$ and $0.05\ k_{\mathrm{B}}T$, given that the experimental grafts were largely composed of nonpolar, aliphatic chains that are expected to exhibit weak interactions amongst themselves and with the nanocubes.[33] The excluded volume size parameter for polymer-nanocube interactions was obtained according to the Lorentz-Berthelot combining rule $\sigma_{\mathrm{pc}} = (\sigma_{\mathrm{cc}} + \sigma_{\mathrm{pol}})/2$.[34] Lastly, the bond stretching and bending parameters associated with the stiffness of the grafts were kept fixed because the segment size σ_{pol} related to the Kuhn length of the chains indirectly accounts for such stiffness effects. A stretching constant of $k_{\mathrm{s}} = 10\ k_{\mathrm{B}}T/\sigma^2$ and $l_0 = \sigma_{\mathrm{pol}}$ provided moderate stretching rigidity to the chains, while a bending constant $k_\theta = 0.1\ k_{\mathrm{B}}T/\mathrm{rad}^2$ with $\theta_0 = 180^\circ$ yielded flexible chains. The complete set of investigated parameters along with their magnitudes are summarized in Table 1.

Free Energy Calculations

To obtain the free energy (PMF) landscape, we computed via MC simulations the ensemble-averaged force $\langle \mathbf{f}(\xi, \theta_1, \theta_2) \rangle$ experienced by one polymer-grafted nanocube from the other as a function of their separation distance ξ for fixed orientations θ_1 and θ_2. The PMF at distance d corresponding to these orientations was then obtained by integrating the x-component of this force (in the direction of the nanocubes' center-to-center axis) from $\xi \to \infty$ to the

required distance $\xi = d$:

$$F(d, \theta_1, \theta_2) = -\int_{\infty}^{d} \langle f_x(\xi, \theta_1, \theta_2) \rangle d\xi. \tag{5}$$

In practice though the PMF was integrated from a finite reference distance by which point the force had decayed to zero. The 3D landscape $F(d, \theta_1, \theta_2)$ was obtained by repeating this calculation for all possible combinations of θ_1 and θ_2.

The configurations of the nanocubes were discretized at a finite resolution to explore all possible orientations and distances. The orientations were varied in 1° increments, and degenerate configurations were avoided by setting the range of angles to $0^\circ \leqslant \theta_1 \leqslant 45^\circ$ and $\theta_1 \leqslant \theta_2 \leqslant 90^\circ - \theta_1$. This choice led to configurations where the right-hand-side nanocube was tilted at a greater angle than the other nanocube. For the integration carried out in Eq. 5, ξ was varied from the contact distance ξ_c to 20σ, where ξ_c is defined as the smallest possible distance that avoided overlap between the nanocubes given by

$$\xi_c = D\left[\frac{1 + \sin(\theta_1 + \theta_2) + \cos(\theta_1 + \theta_2)}{2\cos(\theta_1)}\right] \tag{6}$$

for configurations in which $\theta_2 \geqslant \theta_1$. Since free energies were more sensitive to changes in distance at small surface separations, ξ was changed in increments ranging from 0.1σ to 2σ depending on its magnitude. Overall, a *single* free energy landscape required force calculations (simulations) across ~42,000 nanocube configurations.

To sample conformations of grafted chains for each fixed configuration $(\xi, \theta_1, \theta_2)$, we used the efficient configurational-bias MC method.[35] In this approach, a polymer chain is randomly chosen and regrown in a stepwise manner starting from the bead attached to the nanocube. During regrowth, the position of a bead is picked from a set of randomly generated trial positions with a probability proportional to the Boltzmann factor of the trial. The fully regrown chain generated in this manner is then accepted or rejected according to Rosenbluth weights of the regrown and original chain conformation; these weights ac-

count for the bias introduced by the non-random process of generating chain conformations. This procedure was repeated upto 4 million steps to yield a reasonably-sized ensemble of Boltzmann-distributed conformations for obtaining accurate estimates of $\langle f_x(\xi, \theta_1, \theta_2)\rangle$. A detailed description of this approach and its implementation is given elsewhere.[35,36]

Free Energy Decomposition

For efficient calculation of the energy landscape, the net force f_x experienced by the nanocubes can be broken down into cube- and polymer-mediated portions. The former portion, denoted by $f_{x,\mathrm{cc}}$, remains constant during each simulation carried out at fixed configuration. Hence, even though this force calculation is computationally intensive due to the large number of interatomic force evaluations across the nanocubes, it needs to be carried out only once for each configuration. The fixed configuration also implies zero entropic contribution from this force, and therefore the free energy contributed by $f_{x,\mathrm{cc}}$ is simply equal to the potential energy U_{cc} of cube-cube interactions. While the force $f_{x,\mathrm{pp}}$ arising from polymer-polymer interactions was computed on the fly during the simulation, the force $f_{x,\mathrm{pc}}$ arising from polymer-cube interactions required a prohibitive number of calculations due to the large number of atoms comprising each nanocube. Therefore, we pre-calculated and stored the values of the energies and forces experienced by a "test" polymer bead at discrete grid points around a nanocube, and used linear interpolation to obtain the energies and forces experienced by polymer grafts at their actual positions during the simulation. The overall free energy F was then obtained as $F_{\mathrm{cc}} + F_{\mathrm{pp}} + F_{\mathrm{pc}}$, where the three terms represent contributions from cube-cube, polymer-cube and polymer-polymer interactions obtained via

$$F_{\mathrm{cc}}(d, \theta_1, \theta_2) = U_{\mathrm{cc}}(d, \theta_1, \theta_2) \quad (7)$$

$$F_{\mathrm{pp}}(d, \theta_1, \theta_2) = -\int_{\infty}^{d} \langle f_{x,\mathrm{pp}}(\xi, \theta_1, \theta_2)\rangle d\xi \quad (8)$$

$$F_{\mathrm{pc}}(d, \theta_1, \theta_2) = -\int_{\infty}^{d} \langle f_{x,\mathrm{pc}}(\xi, \theta_1, \theta_2)\rangle d\xi \quad (9)$$

Such dissection of free energy also provided insights into the role of each kind of interaction in governing the eventual stable configuration of the nanocubes. The overall free energy and its polymer-mediated portions can also be decomposed further into entropic and energetic contributions by computing the ensemble-averaged potential energies $\langle U \rangle$, $\langle U_{\rm pc} \rangle$, and $\langle U_{\rm pp} \rangle$. The difference between these potential energies and their corresponding free energies F, $F_{\rm pc}$, and $F_{\rm pp}$ then yields the entropic contributions $T\Delta S$, $T\Delta S_{\rm pc}$, and $T\Delta S_{\rm pp}$.

Results

Orientational phases identified from simulations

One of the goals of this study is to uncover all possible orientational phases exhibited by a pair of polymer-grafted nanocubes. To this end, we computed their free energy landscape $F(d, \theta_1, \theta_2)$ at various points across the parameter space. To ensure that no phase was missed, we explored as many different parameters and as many different combinations of parameter values as was computationally feasible. Specifically, we examined nanocube systems of different sizes D, vdW interaction strengths $\varepsilon_{\rm cc}$, polymer segment excluded volumes (Kuhn lengths) $\sigma_{\rm pol}$, and grafting densities Γ as reported in Table 1. Figure 2a showcases one such energy landscape computed for a representative set of parameters. To identify orientational phases, we determined from each such landscape the global minimum denoting the most stable nanocube configuration.

The complete set of globally stable configurations, identified from all the computed landscapes for the $D = 10\sigma$ nanocubes, is presented in a d-θ_1-θ_2 plot in Fig. 2b. Note that the number of data points in the plot appear to be much fewer that the 960 different systems (landscapes) investigated. The reason is that many of these identified configurations possess the same d, θ_1, and θ_2 values to within the finite resolution of the landscape ($\Delta d = 0.2\sigma$, $\Delta\theta_1 = \Delta\theta_2 = 1^\circ$). We therefore also provide in the plot the populations (when greater than 20) of systems yielding each visible data point. The plot reveals several highly populated

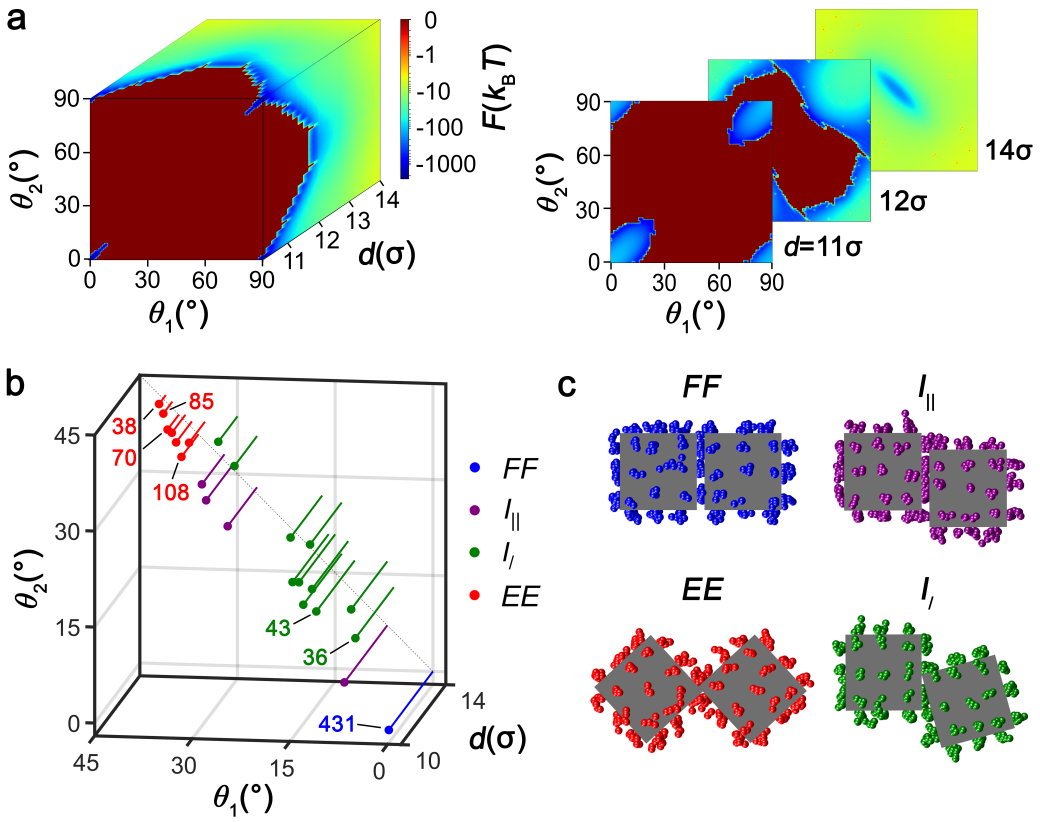

Figure 2: Orientational phases predicted from simulations. (a) Free energy landscape $F(d, \theta_1, \theta_2)$ along with several of its cross-sections shown for one representative set of parameters ($D = 10$, $\varepsilon_{cc} = 2k_BT$, $\Gamma = 0.16/\sigma^2$, $\sigma_{pol} = 0.5\sigma$). This specific nanocube system exhibits a global minimum at $d \approx 10.4\sigma$ and $\theta_1 \approx \theta_2 \approx 0$. (b) Global free-energy minimum configurations for $D = 10\sigma$ nanocubes identified from 960 such landscapes corresponding to different combinations of ε_{cc}, Γ, and σ_{pol}. Configurations are color-coded according to their phase assignment, and populations of configurations greater than 20 are specified within parenthesis. (c) Representative snapshots of the four observed orientational phases: *FF*, $I_{\parallel}$, $I_{/}$, and *EE*.

configurations. The most populated configuration, and also the most isolated in terms of location, resides at $\theta_1 \approx \theta_2 \approx 0$ and $d \approx D$. This configuration clearly corresponds to two nanocubes juxtaposed face to face, which we termed the face-face or *FF* phase in our earlier work. The next most populated configuration resides at $\theta_1 \approx 37°$, $\theta_2 \approx 38°$, and $d \approx 12.6\sigma$, though this configuration does not appear to be as isolated given the presence of many less populated configurations in its vicinity. These configurations appear decidedly less tilted and more compact than the pure edge-edge or *EE* phase with $\theta_1 = \theta_2 = 45°$, and $d \approx 14.1\sigma$ ($= \sqrt{2}D$) considered in our earlier work.[16] Besides these two highly populated

configurations, there also exist a spectrum of less populated configurations located on and off the $\theta_1 = \theta_2$ line symbolizing parallel faces.

Closer inspection of the identified configurations revealed that they can be more effectively categorized based on the fraction of grafts confined between the interacting faces of the nanocubes, as illustrated by their representative snapshots shown in Fig. 2c. In the *FF* phase, representing the most populated configuration discussed above (colored blue in Fig. 2c), *all* of the grafts are enclosed by the interacting faces of the nanocubes. The two faces are fully overlapped, oriented parallel to each other, and separated by a narrow gap just wide enough to accommodate a monolayer of polymer segments. The next most populated configuration, along with several of its neighboring configurations (colored red), also display parallel interacting faces, though their overlap is restricted to small portions near their edges. In fact, the faces exhibit the maximum possible overlap *without* enclosing any polymer segments in between them. Due to the close similarity between these configurations and the idealized edge-to-edge geometry with no overlap, we still call this set of slightly overlapping configurations as the *EE* phase. Note that because the degree of overlap depends on parameters such as the grafting density Γ (which determines the attachment positions of grafts) and the segmental excluded volume σ_{pol}, the *EE* phase displays some spread in the d–θ_1–θ_2 space. The rest of the configurations then represent nanocubes with a *fraction* of grafted chains enclosed in between the interacting faces. These intermediate configurations were further classified into two phases based on the relative orientation of the interacting faces. Configurations with parallel faces were termed as the parallel intermediate phase $I_{\parallel}$ (colored purple), while those with slanted faces were termed the slanted intermediate phase $I_{/}$ (colored green). The above results thus significantly depart from the idealized notions of the *FF* and *EE* phases being the only two stable orientations exhibited by polymer-grafted nanocubes and of the *EE* phase involving touching edges with no overlap.[16,17,37]

Orientational phase diagram predicted by simulations

The relationship between the identified phases and the parameters explored here can be better visualized and understood through a phase diagram. However, a phase diagram constructed *directly* from the putative minimum-free-energy (MFE) configurations presented in Fig. 2b may lead to inaccuracies. Each of these configurations were identified from a *discrete* free energy landscape computed over a coarse 3D grid of $0.2\sigma \times 1^\circ \times 1^\circ$ spacing. While this resolution was adequate for surveying the possible set of stable nanocube configurations and categorizing them into distinct phases, the resolution is too coarse to accurately pinpoint the true location of the global minimum for a given parameter set. The reason is that both vdW and steric interactions vary sharply with the separation distance between nanocubes at close range (Fig. S1). Hence, the free energy of the nanocubes is very sensitive to small changes in their configuration near the global minimum, which typically involves interacting surfaces at close proximity. Consequently, phase diagrams constructed from configurations identified thus far may lead to underestimation of the stability (free energy) of the identified globally stable phase, and in some cases, assignment of an incorrect phase as the globally stable phase. This issue of accuracy could be resolved by using a finer grid, but it would entail prohibitive computational costs. For instance, the landscape was calculated over 42,000 grid points, and using a 5-fold finer grid along each dimensions would increase the number of grid points by a factor of $\sim$125. Using a finer grid locally around the identified phase also will not address the problem for cases where a different phase carries the true global minimum. To this end, we used a distinct strategy that takes advantage of certain observed geometric characteristics of each phase to substantially narrow down the configurational search space required for locating the MFE configuration within each of the four phases. We refer to this reduced set of configurations specific to each phase as "representative configurations".

Representative configurations. Our strategy to obtaining phase diagrams involves reduction of the 3D free-energy landscape $F(d, \theta_1, \theta_2)$ to effectively a 1D free energy landscape

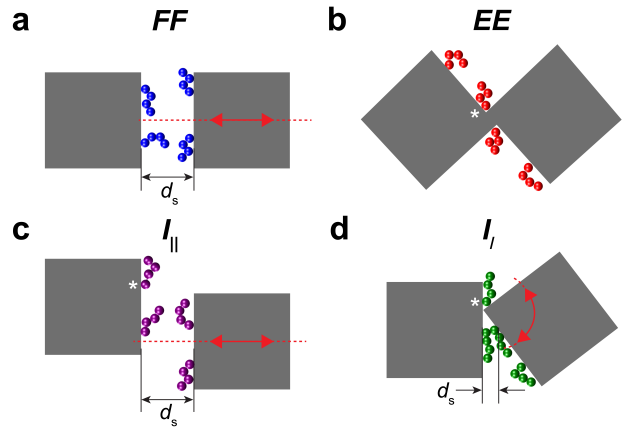

Figure 3: Representative configurations of the (a) *FF*, (b) *EE*, (c) $I_{\|}$, (d) $I_{/}$ phases. The left nanocube was held fixed, and the right nanocube was held fixed (*EE*), translated (*FF* and $I_{\|}$) or rotated ($I_{/}$) as indicated by the red arrows. White asterix represent the graft position on the left nanocube under which the leading edge of the right nanocube rests.

$F^P(x)$ along a judiciously chosen coordinate x unique to each phase P = *FF*, $I_{\|}$, $I_{/}$, or *EE*. In this manner, the 3D search for the global minimum across grid points is reduced to 1D line search across the coordinate x for each phase. This enabled us to more accurately identify the true globally stable phase for constructing our phase diagram and also obtain more accurate free energy values of each phase.

Starting with the *FF* phase, the nanocubes were found to exhibit fully overlapping, parallel faces with $\theta_1 = \theta_2 = 0^\circ$. Furthermore, the interacting faces exhibited the smallest possible separation without excessively squeezing the confined monolayer of graft segments. In this manner, the nanocubes maximized their vdW interactions while avoiding excessive steric repulsion from the confined grafts. Based on these characteristics, the MFE configuration of the *FF* phase was efficiently obtained by restricting the computation of free energies along a coordinate $x = d_s \equiv d - D + \sigma_{cc}$ representing the surface-to-surface separation distance between the interacting nanocube faces, while fixing θ_1 and θ_2 to 0° (Fig. 3a), and then locating the global minimum of the resulting free energy profile $F^{FF}(d_s)$.

The *EE* phase was characterized by parallel, partly overlapping faces close to their edges that are devoid of grafts. To maximize vdW interactions, these "bare" portions overlap to the maximum extent possible in the lateral direction until they press against the first row

of grafted segments and maintain surface contact with each other in the normal direction (Fig. 3b). Based on the *EE* configurations identified in Fig. 2b, we observed that the edges tend to overlap to a distance $d_{\rm exc} \approx 0.3\sigma$ below the attachment point of the first line of grafts, i.e., $d_{\rm overlap} \approx 0.5/\sqrt{\Gamma} - d_{\rm exc}$ (marked by an asterix in the figure). The MFE configuration of the *EE* phase was thus obtained *directly* (without any energy minimization) as the configuration exhibiting $\theta_1 = \theta_2$, contacting surfaces in the normal direction, and lateral overlap of $d_{\rm overlap}$. The associated value of the free energy was denoted by F^{EE}.

Lastly, the phases $I_{\parallel}$ and $I_{/}$ were both characterized by partly overlapping faces that enclose a fraction of the polymer grafts. The former displayed slightly separated, parallel faces to accommodate a monolayer of grafted segments, while the latter exhibited slanted faces with the edge of the slanted face in complete contact with the opposite face to maximize vdW interactions. Given that the grafts were attached in a square pattern, the facing edges could rest under any one of the rows of grafted segments. Hence, we use the notations $I_{\parallel,n}$ and $I_{/,n}$ to denote phases in which the edges fall under the $n^{\rm th}$ row of grafts. As in the case of the *EE* phase, the edges were placed at a small distance $d_{\rm exc} \simeq 0.3\sigma$ below the graft attachment points. The MFE configurations of the $I_{\parallel,n}$ phases were then obtained from the computation, and subsequent minimization, of free energies $F^{I_{\parallel,n}}(d_{\rm s})$ as a function of separation distance $d_{\rm s}$ between the interacting faces, constraining them to be parallel and fixing their edges to distances $d_{\rm exc}$ below the $n^{\rm th}$ line of grafts. The MFE configuration of the $I_{/,n}$ phases were obtained similarly, except that the parallel-face constraint was replaced by the contacting-edge constraint. Furthermore, since the distance between the interacting faces is not constant due to their relative tilt, the free energies $F^{I_{/,n}}(d_{\rm s})$ were computed as a function of a representative separation distance $d_{\rm s}$ defined at the location of the most confined grafted segment in between the two interacting faces. This location was found to be roughly a distance of σ below the grafted position in the identified configurations.

Phase diagram. Using the above approach we determined the MFE configurations and associated free energies of the *FF*, $I_{\parallel}$, $I_{/}$, and *EE* phases for various combinations of $\varepsilon_{\rm cc}$,

σ_{pol}, Γ, and D values, and used the results to generate the phase diagram. Figure 4 presents several 2D cross-sections of the phase diagram at different fixed values of Γ and D, revealing phase behavior as a function of σ_{pol} and $\varepsilon_{\mathrm{cc}}$, two parameters found to most strongly affect nanocube orientations. The nanocubes were observed to form the *FF* phase at large values of $\varepsilon_{\mathrm{cc}}$ (strong attraction between nanocubes) and small values of σ_{pol} (small excluded volume of graft segments), while the *EE* phase is formed under the opposite conditions of small $\varepsilon_{\mathrm{cc}}$ and large σ_{pol}. Sandwiched in between these two phases at intermediate values of $\varepsilon_{\mathrm{cc}}$ and σ_{pol} are the $I_{/}$ and $I_{\parallel}$ phases, with the former occupying most of this remaining parameter space. Comparison of phase diagrams at three different values of the grafting density Γ (Fig. 4a-c) reveals expansion of the $I_{/}$ and $I_{\parallel}$ phases into the surrounding *EE* and *FF* phases with increasing Γ. Interestingly, the $I_{\parallel}$ phase disappears at the smallest grafting density of $\Gamma = 0.04$ (Fig. 4a). Comparison of phase diagrams at two different nanocube sizes D (Fig. 4a,d) revealed an equally intriguing disappearance of the $I_{/}$ and $I_{\parallel}$ phases in large nanocubes ($D = 20$; Fig. 4d). Note that we explored only those regions of the parameter space that lead to assembly, that is, sufficiently large values of $\varepsilon_{\mathrm{cc}}$. Smaller values would lead to repulsive or weakly attractive free energies for all phases, so the nanocubes would prefer to remain dispersed.

The phase behavior observed here must arise from an interplay between attractive vdW interactions across the nanocubes and repulsive steric interactions from the grafted chains squeezed in between the nanocubes. vdW interactions *alone* would cause the nanocubes to assemble into the *FF* phase with contacting faces, and so steric repulsion must be responsible for the tilting and/or sliding of the nanocubes relative to each other required to form the $I_{\parallel}$, $I_{/}$, and *EE* phases. To investigate this interplay, we examined the free energy F^P and its contributions F^P_{cc} and $F^P_{\mathrm{pol}} \equiv F^P_{\mathrm{pp}} + F^P_{\mathrm{pc}}$ arising from vdW and steric interactions for nanocubes yielding distinct phases. We chose *three* different nanocube systems, denoted by "N1", "N2", and "N3" in Fig. 4c, which differ in σ_{pol} and $\varepsilon_{\mathrm{cc}}$ and yield the *FF*, $I_{/}$, and *EE* phases, respectively. We then compared the free energies of the three systems exhibiting

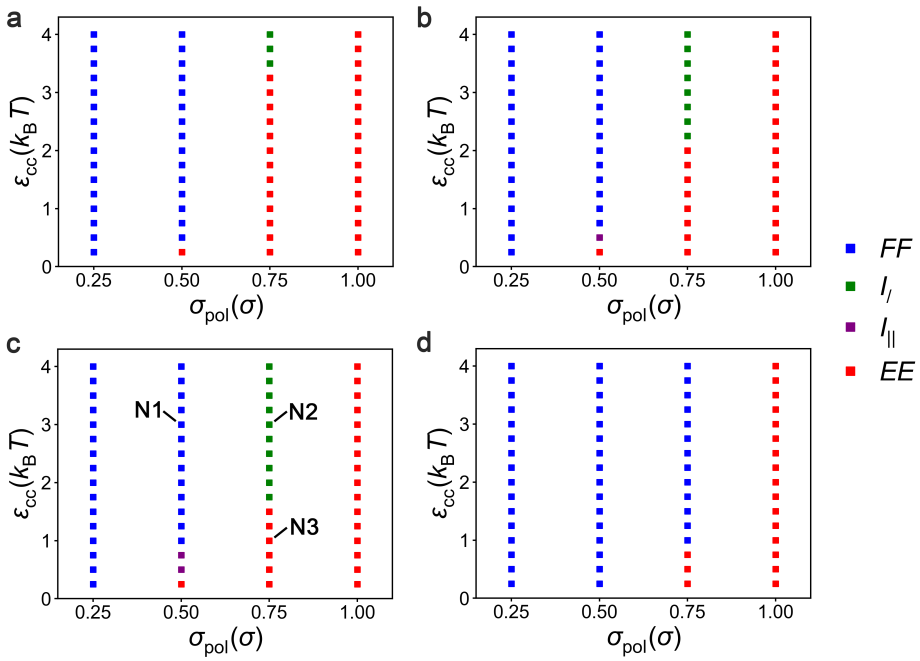

Figure 4: Orientational phase diagram obtained from simulations. Cross-sections of the phase diagram along $\sigma_{\rm pol}$ and $\varepsilon_{\rm cc}$ at fixed values of (a) $D = 10\sigma$, $\Gamma = 0.04/\sigma^2$, (b) $D = 10\sigma$, $\Gamma = 0.09/\sigma^2$, (c) $D = 10\sigma$, $\Gamma = 0.16/\sigma^2$, and (d) $D = 20\sigma$, $\Gamma = 0.04/\sigma^2$.

representative configurations of the *FF*, $I_/$, and *EE* phases, noting that only one of them represents the globally stable phase of each system.

Figure 5a-c presents a comparison of the free energies $F^{FF}(d_{\rm s})$, $F^{I_/}(d_{\rm s})$, and F^{EE}, of the three phases, and of their vdW contributions $F_{\rm cc}^{FF}(d_{\rm s})$, $F_{\rm cc}^{I_/}(d_{\rm s})$, $F_{\rm cc}^{EE}$ and steric contributions $F_{\rm pol}^{FF}(d_{\rm s})$, $F_{\rm pol}^{I_/}(d_{\rm s})$, and $F_{\rm pol}^{EE}$, respectively. As expected, the two free energy contributions are of opposite sign with $F_{\rm cc}^{P} < 0$ and $F_{\rm pol}^{P} > 0$, and the overall free energies F^P of the three nanocubes at the energy minimum are indeed the lowest (most favorable) for the configuration representing their stable phase, i.e., *FF*, $I_/$, and *EE* for N1, N2, and N3. Furthermore, the *magnitudes* of $F_{\rm cc}^{P}$ and $F_{\rm pol}^{P}$ decrease in the order $FF > I_/ > EE$, trends that easily explained by the representative snapshots of nanocube phases shown in Fig. 2c: $F_{\rm cc}^{P}$ is expected to correlate with the surface area of the nanocube faces in close proximity to each other (due to the sharp decay of vdW interactions with distance), and the amount of overlap between the interacting faces indeed decreases in the same sequence for the three phases as the computed $F_{\rm cc}^{P}$; In similar vein, $F_{\rm pol}^{P}$ should correlate with the number of graft

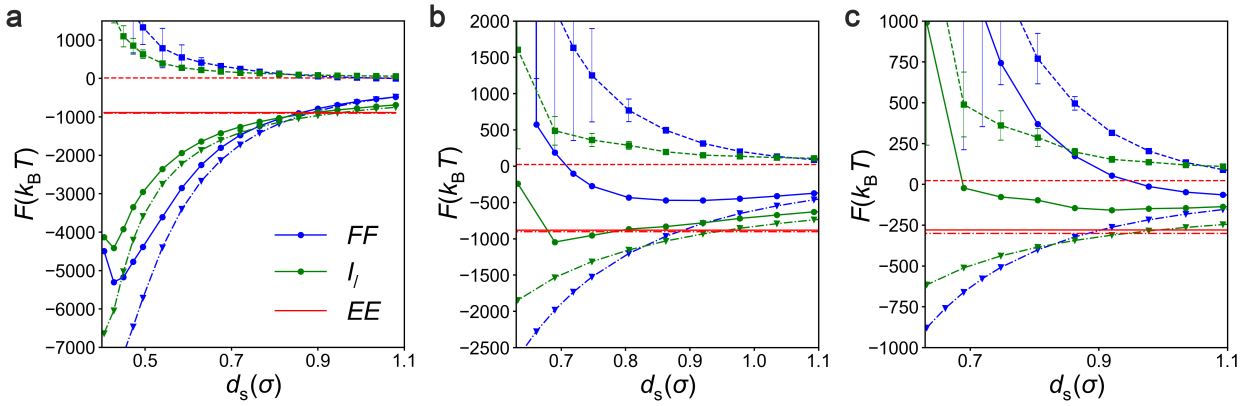

Figure 5: Role of vdW and steric interactions in governing orientational phase behavior. Free energy contributions from vdW attraction (dash-dotted lines) and steric repulsion (dashed lines) to the overall free energy (solid lines) plotted as a function of surface separation distance d_s for the *FF* (blue), $I_/$ (green), and *EE* (red) representative configurations. The free energies are plotted for the three nanocube systems labelled N1, N2, and N3 in Fig. 4c of same size and grafting density ($D = 10\sigma$, $\Gamma = 0.16/\sigma^2$) but different polymer excluded volumes and/or nanocube attraction strengths: (a) $\sigma_{\rm pol} = 0.5\sigma$ and $\varepsilon_{\rm cc} = 3\ k_{\rm B}T$ (N1), (b) $\sigma_{\rm pol} = 0.75\sigma$ and $\varepsilon_{\rm cc} = 3\ k_{\rm B}T$ (N2), and (c) $\sigma_{\rm pol} = 0.75\sigma$ and $\varepsilon_{\rm cc} = 1\ k_{\rm B}T$ (N3).

segments confined between the interacting faces, and the number of such confined chains decreasing in the same sequence for the three phases as $F^P_{\rm pol}$.

We next turn to *differences* in the strengths of vdW and steric interactions across N1, N2, and N3 to explain how this interplay between the two interactions yields distinct phases for the three systems (Fig. 5). For N1 with small $\sigma_{\rm pol} = 0.5\sigma$ (Fig. 5a), the *FF* configuration exhibits the strongest steric repulsion $F^P_{\rm pol}$ as well as the strongest vdW attraction $F^P_{\rm cc}$ amongst the three configurations. However, due to the small excluded volume of the grafted polymer segments, the steric interactions are weak compared to vdW interactions for all configurations. Therefore, in this "surface interactions-dominated" regime, the *FF* configuration with the strongest vdW interactions ends up yielding the deepest minimum in the *overall* free energy profiles F^P amongst the three configurations. In other words, the weak steric repulsion here allows the two nanocubes to come into closer proximity ($d_s \approx 0.4\sigma$), allowing them to avail of the strong vdW interactions provided by the *FF* configuration. This situation is reversed for N3 with large $\sigma_{\rm pol} = 0.75\sigma$ and small $\varepsilon_{\rm cc} = 1k_{\rm B}T$ (Fig. 5c), where the large excluded volume of the graft segments leads to strong steric repulsion for

all configurations, *except* the *EE* configuration which does not confine any polymer chains in between its contacting faces. Hence, in this "polymer interactions-dominated" regime, the *EE* configuration which does not contain any confined grafts and exhibits negligible steric repulsion ends up exhibiting the most favorable overall free energy. In fact, the strong steric repulsion pushes the *FF* and $I_{/}$ nanocubes apart to separations where the vdW interactions become even weaker than that of the *EE* configuration. Finally, for N2 possessing grafts with large $\sigma_{\mathrm{pol}} = 0.75\sigma$ and large $\varepsilon_{\mathrm{cc}} = 3k_{\mathrm{B}}T$ (Fig. 5b), vdW and steric interactions are more or less equally strong (except for the *EE* configuration where steric repulsion remains weak). In this intermediate regime, the $I_{/}$ configuration yields the lowest interaction free energy of the three configurations, providing a compromise between the *FF* configuration, which yields strong vdW interactions but still suffers from strong steric repulsion, and the *EE* phase, which consistently yields weak steric repulsion and weak vdW interactions.

The above analysis illustrates how the interplay between vdW and steric interactions yields the observed sequence of *FF*, $I_{/}$, and *EE* phases with increasing σ_{pol} and decreasing $\varepsilon_{\mathrm{cc}}$ in Fig. 4. In particular, increasing the magnitude of σ_{pol}, which controls the strength of polymer-mediated steric interactions between the nanocubes, causes them to go from a surface interactions-dominated regime, where phases that *maximize* vdW interactions are preferred, to a polymer interactions-dominated regime, where phases that *minimize* steric interactions are preferred. The same argument can be used to explain the opposite sequence of phases (*EE* to $I_{/}$ to *FF*) observed upon increasing $\varepsilon_{\mathrm{cc}}$. This parameter controls the strength of vdW interactions between the nanocubes, and an increase in the magnitude of $\varepsilon_{\mathrm{cc}}$ should cause the system to go from a regime dominated by polymer interactions to a regime dominated by surface interactions, the opposite of what is observed with increasing σ_{pol}. However, these simple reasonings are unable to explain the observed broadening of the $I_{/}$ phase with increasing grafting density Γ, the small size and location of the $I_{\|}$ phase, or the complete disappearance of both $I_{/}$ and $I_{\|}$ with increasing size of the nanocubes. These effects will be explained with the scaling expressions developed below.

Free-energy scaling relations

We next formulated *analytical* expressions for the free energy profiles $F^{FF}(d_s)$, $F^{I_\parallel}(d_s)$, $F^{(I_/)}(d_s)$, and F^{EE} computed earlier from simulations for each phase for different values of parameters D, ε_{cc}, σ_{pol}, and Γ. The motivation for developing such an analytical framework was three-fold: to provide new and deeper insights into the morphology of the orientational phase diagrams shown in Fig. 4; to allow interpolation and extrapolation of free energies to a wider range of conditions than explored by simulations for generating a more complete phase diagram; and to provide researchers a more rapid and accessible means to predicting phase diagrams that does not involve performing costly simulations. In the following sections, we develop analytical scaling relationships for the free energy contributions F^P_{cc}, F^P_{pp}, and F^P_{pc} arising from vdW, polymer-cube, and polymer-polymer interactions, whose summation should then yield the overall free energy profiles F^P we seek.

vdW interactions. The free-energy contribution F^P_{cc} from vdW interactions is expected to vary not only with separation distance d_s, size D, and energy parameter ε_{cc}, but also grafting density Γ, which determines the amount of overlap between the nanocube faces in the $I_\parallel$, $I_/$, and *EE* phases. While F^P_{cc} clearly scales linearly with ε_{cc}, its dependence on the remaining parameters is not so obvious. To obtain these other dependencies, we analyzed the variation of F^P_{cc} with distance d_s for different values of D and Γ, noting that the distance dependence only applies to the *FF*, $I_\parallel$, $I_/$ phases, and not the *EE* phase where the MFE configuration is already known to be the contact distance. The vdW energies were computed by summing the LJ interactions (with $\varepsilon_{cc} = 1\ k_BT$) across all pairs of atoms comprising the two nanocubes.

Figure 6 presents representative plots showing the dependence of F^P_{cc} on d_s for the four phases and the variation of these $F^P_{cc}(d_s)$ profiles with size D for one of the phases (*FF*); additional plots showing dependence on Γ and D are provided in Fig. S1. Since nanocubes exhibit short separation distances at the MFE configuration in each phase (see Figs. 2 and 5), the vdW energies need to be plotted over only small distances d_s. Importantly, this

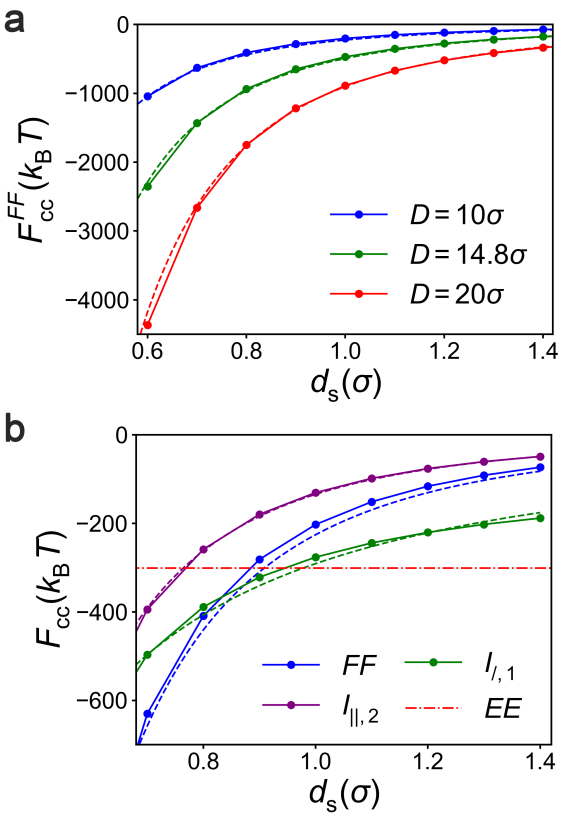

Figure 6: vdW interaction energy F_{cc}^{P} as a function of surface separation distance d_s. Results are plotted for (a) FF phase for nanocubes of sizes $D = 10$, 14.8, and 20σ; and (b) all phases of $D = 10\sigma$ nanocubes with $\Gamma = 0.16/\sigma^2$. Solid lines (and symbols) represent computed values and dashed lines are fits to this data using a power-law. F_{cc}^{EE} is plotted as a fixed value corresponding to contact distance.

allows us to obtain simple and accurate power-law scaling relationships between F_{cc}^{P} and d_s that only need to be valid over this short range of relevant distances. We found that the computed vdW energies could be well described by the following scaling relationship:

$$F_{cc}^{P} = -c\varepsilon_{cc}D^{\alpha}d_s^{-\beta}, \tag{10}$$

where $\alpha > 0$ is a scaling exponent that accounts for the increase in vdW energy with size D; $\beta > 0$ is another scaling exponent that accounts for the decay in the strength of vdW forces with distance d_s; and c is a coefficient that captures the dependence on grafting density and also provides quantitative agreement with computed interaction energy. The obtained values

Table 2: Values of coefficients and exponents of the analytical free energy model derived in this study for the four orientational phases†:

Phase	c	α	β	n_{conf}
FF	2.256	2	3	$2\Gamma D^2$
$I_{\parallel,n}$	$2.256\gamma_{\mathrm{cc}}$	2	3	$2(n_{\mathrm{s}}-n)D\sqrt{\Gamma}$
$I_{/,1}, \Gamma = 0.04$	40.49	1	1.5	$2D\sqrt{\Gamma}$
$I_{/,1}, \Gamma = 0.09$	33.33	1	1.5	$2D\sqrt{\Gamma}$
$I_{/,2}, \Gamma = 0.09$	30.28	1	1.5	$2D\sqrt{\Gamma}$
$I_{/,1}, \Gamma = 0.16$	29.1	1	1.5	$2D\sqrt{\Gamma}$
$I_{/,2}, \Gamma = 0.16$	27.69	1	1.5	$2D\sqrt{\Gamma}$
$I_{/,3}, \Gamma = 0.16$	24.97	1	1.5	$2D\sqrt{\Gamma}$
EE	$\gamma_{\mathrm{cc}} F_{\mathrm{cc}}^{FF}(\mathrm{contact})$	2	0	0

$$^{\dagger}F_{\mathrm{tot}} = -c\varepsilon_{\mathrm{cc}}D^{\alpha}d_{\mathrm{s}}^{-\beta} + 15.0n_{\mathrm{conf}}\sigma_{\mathrm{pc}}^{3}\varepsilon_{\mathrm{pc}}\left[d_{\mathrm{n}}^{-12} - d_{\mathrm{n}}^{-6}\right] + 6.52n_{\mathrm{conf}}d_{\mathrm{n}}^{-2.82}$$

of α, β, and c are summarized in Table 2.

The tabulated values reveal similar size and distance scalings, albeit with different coefficients, for the FF, $I_{\parallel}$ and EE phases exhibiting *parallel* nanocubes. First, F_{cc}^{P} scales as D^2 for these phases, which may be explained as follows. At the small separation distances d_{s} of interest in this study, most lattice atoms comprising the two nanocubes interact at distances much larger than σ_{cc}, the characteristic range of the LJ potential underlying vdW interactions. Hence, F_{cc}^{P} is dominated by local interactions across lattice atoms at or close to the two facing surfaces of the nanocubes. As a result, the size scaling is proportional to the area of the overlapped surfaces of the two nanocubes. By similar reasoning, $F_{\mathrm{cc}}^{I_{\parallel}}$ and F_{cc}^{EE} should be smaller than F_{cc}^{FF} (at equivalent d_{s}) by a proportionality factor γ_{cc} equal to the fraction of overlap between the interacting surfaces of the nanocubes in the two phases. For instance, $F_{\mathrm{cc}}^{(I_{\parallel},2)}$ for nanocubes with $\Gamma = 0.16/\sigma^2$ exhibiting 59.5% overlap between their surfaces is equal to $0.595 \times F_{\mathrm{cc}}^{FF}$ at equivalent d_{s}. Our choice of grafting an integer number n_{s} of chains per side of a nanocube leads to a γ_{cc} of

$$\gamma_{\mathrm{cc}} = \frac{D - \frac{n-0.5}{\sqrt{\Gamma}} - d_{\mathrm{exc}}}{D}, \tag{11}$$

where $n = 1, \cdots, n_s - 1$ for the $I_{\parallel,n}$ phases, and $n = n_s$ for the *EE* phase. Note that F_{cc}^{EE} is also dependent on Γ. Second, F_{cc}^{P} scales as d_s^{-3} for the three phases. Note however that the distance scaling exponent for the *EE* phase is listed as $\beta = 0$ in Table 2 to imply that its MFE configuration has already been established to exhibit contact distances ($d_s = 0$). Theoretically, the vdW interaction energy between two infinitely *thin* surfaces is expected to scale as d^{-4} with separation distance d, whereas that between two infinitely *thick* surfaces (half-planes) is expected to scale as d^{-2}.[38] It therefore seems reasonable that our *finite*-sized nanocubes, which are neither infinitely thin nor infinitely thick, exhibit an intermediate distance scaling of d_s^{-3}. We emphasize at this juncture that the observed distance scalings for all nanocube phases are meant to be approximate and valid only for the short range of small separation distances relevant for assembly.

The scaling behavior of F_{cc}^{P} is vastly different for the $I_{/}$ phase. First, it scaled linearly and not quadratically with D (Fig. S1). In this phase, one edge of the nanocube is in contact with the face of the other nanocube. Given that lattice atoms separated by distances much larger than σ_{cc} exhibit negligible vdW interactions, only interactions mediated by the contacting edge of the nanocube and the lattice atoms in its immediate vicinity contribute to $F_{cc}^{I_{/}}$. Therefore, $F_{cc}^{I_{/}}$ scales with the length and not the surface area of the nanocube face. In addition, the coefficient c denoting magnitude of vdW interactions was found to be affected, albeit weakly, by the position of the contacting nanocube edge. In general, the magnitude of c increased with increasing "projected" overlap between the facing surfaces of the two nanocubes, and hence, c decreased with increasing n of $I_{/,n}$. Second, we observed a distance scaling exponent $\beta = 1.5$ for the $I_{/}$ phase, as opposed to $\beta = 3$ observed for the remaining three phases with parallel faces. This was because the distances between the lattice atoms were affected differently by the changes in d_s depending on their positions. For atoms at the contacting edge, changes in d_s had no effect on their interparticle distances, and β was effectively zero for these atoms. However, for atoms at the location used for defining the nanocube separation distance, the distances from the other nanocubes surfaces were

equivalent to d_s. For these atoms, changes in d_s had a similar effect on $F_{cc}^{I/}$ as they did for the other phases, and hence $\beta \approx 3$. The combined effect of such position-dependent scalings likely leads to the observed scaling of $\beta = 1.5$.

The observed differences in the vdW distance scalings β and coefficients c of the phases implies that the phase with the strongest favorable F_{cc}^{P} depends on d_s, as demonstrated in Fig. 6b. When d_s is small, the *FF* phase exhibits the strongest vdW energy, as expected. However, because F_{cc}^{FF} decays more sharply with d_s than $F_{cc}^{I/}$, the vdW energy of the *FF* phase is eventually surpassed by that of the $I_/$ phase as d_s increases. Upon further increase in d_s, the vdW energy of the *EE* phase surpasses that of all other phases, as nanocubes always remain in contact in this phase.

Polymer-surface interactions. We next investigated the free-energy contribution F_{pc}^{P} arising from polymer-cube interactions, beginning with that of the *FF* phase. To this end, we varied ε_{pc}, σ_{pol}, and Γ expected to affect this interaction and examined the effect of each parameter on the distance-dependent $F_{pc}^{FF}(d_s)$ profiles computed from simulations. As the primary effect of the grafted chains is the steric hindrance they impose through the excluded volume of their segments, the impact of the nanocube separation distance on F_{pc}^{FF} could be conveniently represented in terms of a normalized separation distance d_n given by (see Fig. S2):

$$d_n = \frac{d_s}{2\sigma_{pc}}. \tag{12}$$

In addition, we found that the behavior of F_{pc}^{FF} could be better modeled by decomposing it into its energetic and entropic components, denoted by U_{pc}^{FF} and $-T\Delta S_{pc}^{FF}$, and separately examining their variation with the aforementioned parameters, which modulated the two components in very different ways. For instance, Fig. 7a depicts F_{pc}^{FF} and its two components computed for a representative system with $\Gamma = 0.16/\sigma^2$, $\varepsilon_{pc} = 0.1k_BT$, and $\sigma_{pol} = 0.75\sigma$, and it can be observed that U_{pc}^{FF} decays more strongly with d_n than $-T\Delta S_{pc}^{FF}$.

By analyzing the variation of U_{pc}^{FF} with ε_{pc}, σ_{pol}, and Γ, as shown in Fig. 7d-f, we arrived

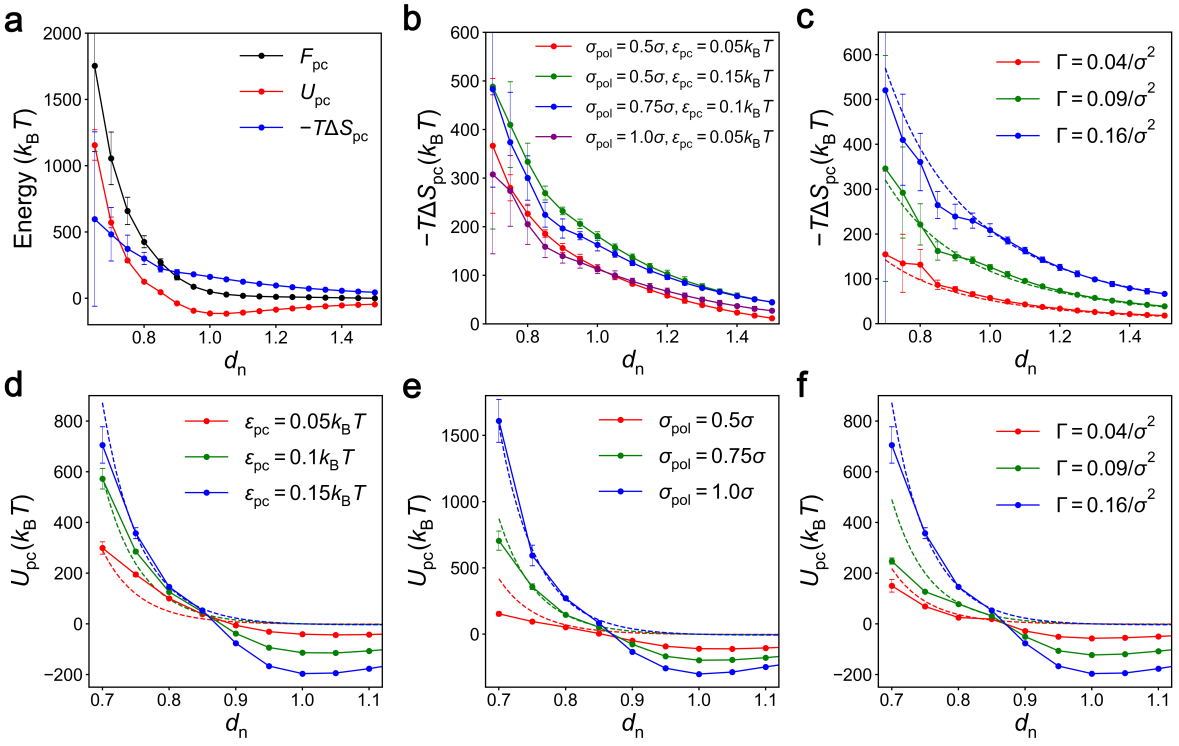

Figure 7: Polymer-nanocube interaction free energies F_{pc}^{P} of the FF phase as a function of normalized separation distance d_{n}. (a) Decomposition of free energy into potential energy and entropy contributions for nanocubes with $\varepsilon_{\mathrm{pc}} = 0.1\ k_{\mathrm{B}}T$. (b–c) Dependence of the entropic contribution on interaction parameters σ_{pol} and $\varepsilon_{\mathrm{pc}}$ (b), and grafting density Γ (c). (d–f) Dependence of potential energy contribution on $\varepsilon_{\mathrm{pc}}$ (d), σ_{pol} (e), and Γ (f). The nanocube parameters were set at $\Gamma = 0.16/\sigma^2$, $\sigma_{\mathrm{pol}} = 0.75\sigma$, $\varepsilon_{\mathrm{pc}} = 0.15\ k_{\mathrm{B}}T$ unless otherwise specified.

at the following simplified description of the potential energy:

$$U_{\mathrm{pc}}^{FF} = 15.0 n_{\mathrm{conf}} \sigma_{\mathrm{pc}}^{3} \varepsilon_{\mathrm{pc}} \left[d_{\mathrm{n}}^{-12} - d_{\mathrm{n}}^{-6} \right], \tag{13}$$

where n_{conf} denotes the number of confined polymer chains given by $2\Gamma D^2$. The above expression indicates that U_{pc}^{FF} is linearly proportional to n_{conf} and $\varepsilon_{\mathrm{pc}}$, and also scales like the LJ potential with respect to d_n. Thus, the overall potential energy of interactions between the polymer grafts and nanocubes is given by the sum of LJ interactions between each polymer segment with the outermost lattice atoms of the nanocube. Given that the *ensemble-averaged* potential energy exhibits the same functional form as the underlying pair potential suggests

that other interactions such as those between the segments do not significantly affect the effective interactions between the polymer and the nanocube. The origin of $U_{\rm pc}^{FF} \sim \sigma_{\rm pc}^3$ dependence is less straightforward to explain. This scaling likely occurs from our treatment of nanocubes as a simple-cubic lattice of LJ atoms. This results in an atomically corrugated nanocube surface, which causes the grafted chain segments confined in between nanocubes to experience an uneven confinement volume. Consequently, polymer segments with small $\sigma_{\rm pc}$ are better able to accommodate within the cavities in between lattice atoms to lower the interatomic LJ repulsion as compared to large segments (see Fig. S3).

The entropic contribution $-T\Delta S_{\rm pc}^{FF}$ was found to exhibit a weak dependence on $\varepsilon_{\rm pc}$, almost no dependence on $\sigma_{\rm pc}$ after normalization, and a strong dependence on $n_{\rm conf}$, as shown on Fig. 7b-c. The magnitude of this contribution was found to be reasonably described by

$$-T\Delta S_{\rm pc}^{FF} = 6.52 n_{\rm conf} d_{\rm n}^{-2.82}, \tag{14}$$

where the linear dependence on $n_{\rm conf}$ (as in the case of $U_{\rm pc}^{FF}$) indicates additivity of entropic contributions from the confined grafts, and the inverse power-law dependence on distance is consistent with the expected increase in entropy loss with increasing confinement, though the physical basis for the observed -2.82 scaling exponent remains unknown.

Interestingly, Eqs. 13 and 14 proposed for the *FF* phase *also* provide good approximations for the polymer-surface interactions of the $I_{\parallel}$, $I_{/}$, and *EE* phases, with the *only* distinction being the fewer number $n_{\rm conf}$ of grafted chains these phases confine compared to the *FF* phase (see Table 2). This is demonstrated and further investigated in Fig. 8. Figure 8a depicts the $F_{\rm pc}^{P}(d_{\rm n})$ profiles computed for the $I_{\parallel,n}$ phases (n = 1, 2, and 3) and the *EE* phase for nanocubes with $\Gamma = 0.16/\sigma^2$. Clearly, the magnitude of steric repulsion for these phases decreases in the same order as decreasing polymer confinement: $I_{\parallel,1} > I_{\parallel,2} > I_{\parallel,3} > EE$. Moreover, the ratios of $F_{\rm pc}^{P}$ for the four phases to that of the *FF* phase approximately equal the ratios of the number of chains $n_{\rm conf}$ they confine. For example, $n_{\rm conf}$ for the $I_{\parallel,2}$ phase is

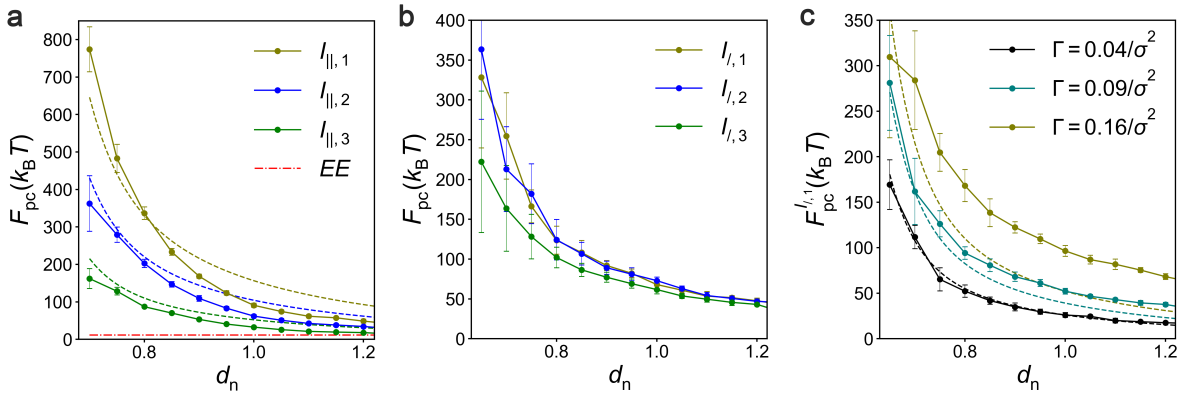

Figure 8: Polymer-nanocube interaction free energies $F_{\rm pc}^P$ as a function of normalized separation distance $d_{\rm n}$ for: (a) $I_{\parallel,n}$ and EE phases, (b) $I_{/,n}$ phases, and (c) $I_{/,1}$ phase at three different values of Γ. The nanocube parameters were set to $\sigma_{\rm pol} = 0.75\sigma$, $\varepsilon_{\rm pc} = 0.05\ k_{\rm B}T$, $\Gamma = 0.16/\sigma^2$, unless otherwise specified.

half of that of FF and $F_{\rm pc}^{I_{\parallel},2} \approx 1/2 \times F_{\rm pc}^{FF}$; and $n_{\rm conf}$ of the EE phase is zero and $F_{\rm pc}^{EE} \approx 0$. More generally, $n_{\rm conf}$ is equal to $2(n_{\rm s} - n)D\sqrt{\Gamma}$ for the $I_{\parallel,n}$ phases. Figure 8b depicting $F_{\rm pc}^{FF}(d_{\rm n})$ profiles for the $I_{/,n}$ phases (n = 1, 2, and 3) at the same grafting density reveal much smaller differences across the three phases. This is understandable given that *only* the closest row of grafted chains below the contacting edge of the nanocubes are strongly confined and contribute significantly to $F_{\rm pc}^P$. The contact position of the nanocube edge, therefore, does not significantly impact $F_{\rm pc}^P$. The $F_{\rm pc}^P$ for the $I_{/,n}$ phases should then scale as $2D\sqrt{\Gamma}$, the number of grafted chains in a single row. Indeed, $F_{\rm pc}^P$ profiles computed for the $I_{/,1}$ phase at different values of Γ confirms this square-root dependence on the grafting density (Fig. 8c). In addition to capturing the $n_{\rm conf}$-dependence for the $I_{\parallel}$ and $I_{/}$ phases, Figs. 8a–c also importantly demonstrate that the model provides reasonable predictions of the distance dependence of $F_{\rm pc}^P$.

Polymer-polymer interactions. Finally, we investigated the behavior of the free energy contribution $F_{\rm pp}^P$ arising from polymer-polymer interactions. Figure 9a shows typical behavior with respect to distance $d_{\rm s}$ for the FF phase. Unlike polymer-surface interactions, where contributions from potential energies are significant, $F_{\rm pp}^{FF}$ is dictated almost entirely by entropy. This trend was observed even when $\varepsilon_{\rm pp}$ was increased ten-folds to 1.0 $k_{\rm B}T$. Fur-

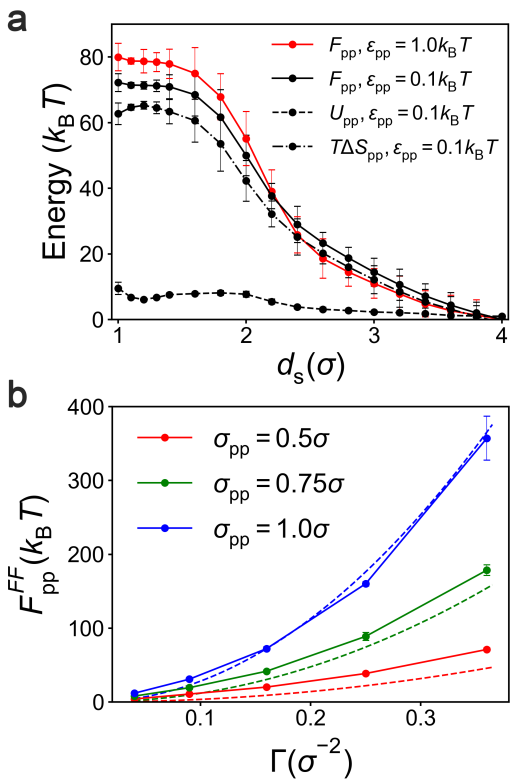

Figure 9: Polymer-polymer interaction free energies $F_{\rm pp}^{FF}$. (a) Decomposition of $F_{\rm pp}^{FF}$ (solid) into potential energy $U_{\rm pp}^{FF}$ (dashed) and entropy $-T\Delta S_{\rm pp}$ (dash-dot). (b) $F_{\rm pp}^{FF}$ within the terminal region.

thermore, we observed that $F_{\rm pp}^{FF}$ repulsion rose steadily with increasing confinement before plateauting off at distances $\lesssim 1.7\sigma$. In this "terminal" region, the confined grafted chains were compressed into monolayers and their conformations within the monolayer were entirely governed by polymer-surface interactions, explaining why further reduction in the confinement does not induce further increase in $F_{\rm pp}^{FF}$. As all nanocube phases displayed small $d_{\rm s}$, we only examined $F_{\rm pp}^{FF}$ in terminal regions.

The magnitude of $F_{\rm pp}^{FF}$ was further examined as a function of grafting density Γ and $\sigma_{\rm pp}$ in Fig. 9b. The observed behavior can be well described by

$$F_{\rm pp}^{FF} = 28.21\sigma_{\rm pp}^3 D^2\Gamma^2. \tag{15}$$

Unlike $F_{\rm pc}^{FF}$ which scaled linearly with Γ, $F_{\rm pp}^{FF}$ was found to scale quadratically with Γ.

The reason is that $F_{\rm pp}^{FF}$ involves *pairwise* interactions between polymer segments, and the number of segments contributed by each nanocube within the confined volume in between them is proportional to Γ. However, $F_{\rm pp}^{FF}$ still scales as D^2 (Fig. S1). This is because the radius of gyration of the grafts is much shorter than D, and therefore, the polymer-polymer interactions mediated by each grafted chain are localized about its attachment position rather than across the entire face of the nanocube. Lastly, $F_{\rm pp}^{FF}$ was found to be proportional to the volume of the polymer segments. As the grafted chains are squeezed into monolayers, the volume occupied by each chain is proportional to the volume of its segments. Therefore, the entropy of the polymer chain confinement, which played the dominant role in determining $F_{\rm pp}^{FF}$, was proportional to $\sigma_{\rm pp}^3$.

It should be noted that even though $F_{\rm pp}^{FF}$ scaled quadratically with Γ, its magnitude was still negligible compared to $F_{\rm pc}^{FF}$. For example, assuming $d_{\rm n}$ of 0.7 and $\sigma_{\rm pol}$ of 1.0σ, Γ would have to be $\gtrsim 2.4/\sigma^2$ (exceeding the close-packed density) for $F_{\rm pp}^{FF}$ to equal the magnitude of $F_{\rm pc}^{FF}$. The polymer-polymer interactions are even weaker for the $I_{/}$ and $I_{\parallel}$ phases and negligible for the *EE* phase. Therefore, for constructing phase diagrams based on the free energies of the different phases, we *ignored* the small contribution from polymer-polymer interactions.

Orientational phase diagram from scaling relationships

We next constructed an orientational phase diagram using the functional forms of the free energies developed above. These free-energy expressions $F^P(d_{\rm s})$ summarized in Table 2 for all four phases are functions of the separation distance $d_{\rm s}$. The free energy of a phase is given by the global minimum denoted by $F_{\rm m}^P$, which can be obtained by solving $\partial F^P/\partial d_{\rm s} = 0$, a $13^{\rm th}$ order polynomial function; the separation distance at the minimum denoted by $d_{\rm m}^P$ represents the "equilibrium" configuration of the phase. Phase boundaries occur when two different phases exhibit equivalent $F_{\rm m}^P$ for the same set of nanocube parameters. Instead of numerically solving for these boundaries, we obtained the phase diagram by calculating $F_{\rm m}^P$ for each phase

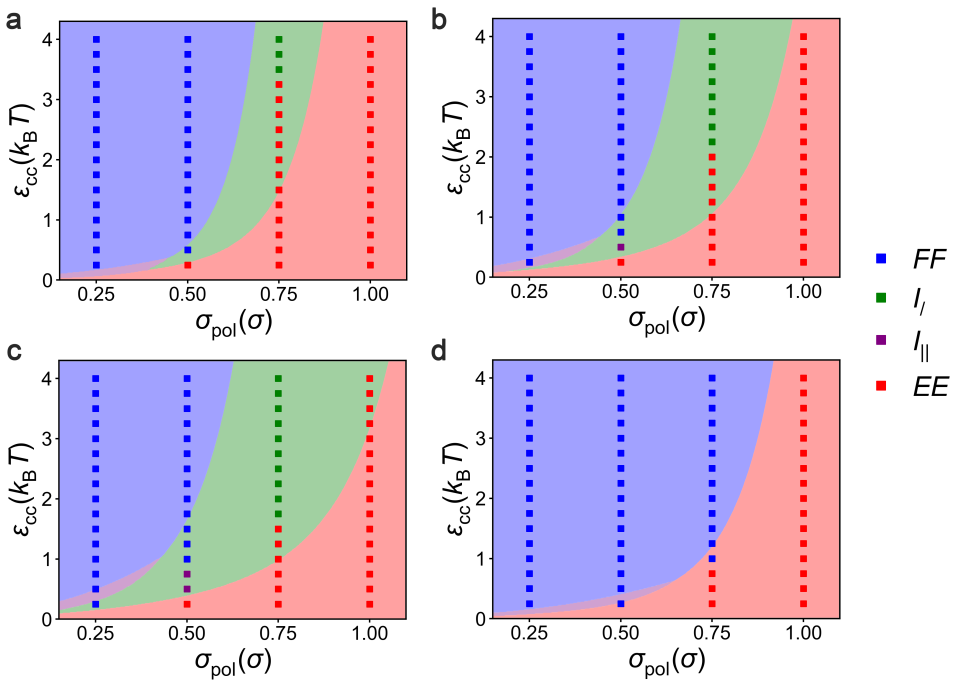

Figure 10: Orientational phase diagram obtained from free-energy scaling relationships. Cross-sections of the phase diagram in the σ_{pol}-ε_{cc} space with (a) $\Gamma = 0.04/\sigma^2$, (b) $\Gamma = 0.09/\sigma^2$, (c) $\Gamma = 0.16/\sigma^2$ for $D = 10\sigma$ nanocubes, and (d) $\Gamma = 0.04/\sigma^2$ for $D = 20\sigma$ nanocubes.

over a finely-spaced grid spanning the desired parameter space, and then assigning phases to each grid point based on the phase possessing the lowest F_{m}^{P}. Figure 10a–d shows various cross-sections of the resulting phase diagram depicting phase behavior as a function of σ_{pol} and ε_{cc} at four different fixed values of Γ and D. For comparison, we also included within each plot the corresponding phase behavior obtained earlier from simulations.

The phase diagram obtained from scaling analysis displayed similar morphology and trends as those computed from simulations, and the scaling relations helped explain many of these features of the phase diagram, several of which were not resolvable by simulations. First, the phases changed in the order $FF \rightarrow I_{/} \rightarrow EE$ with increasing σ_{pol} or decreasing ε_{cc}. While this effect was already well explained by the interplay between the simulated vdW and steric interactions (Fig. 5), the scaling relations provide additional insight into the phase transitions. In particular, the relations show how increasing σ_{pol}, or decreasing ε_{cc}, increases the *relative* magnitude of the steric to vdW interaction terms, which in turn increases the

equilibrium distance $d^P_{\min}$ in all phases, except the *EE* phase where d_s is considered fixed. Since the vdW energy term F^P_{cc} decays the sharpest with distance for the *FF* phase (scaling exponent $\beta = 3$), weaker for the $I_/$ phase ($\beta = 1.5$), and the weakest for the *EE* phase ($\beta = 0$), the increase in $d^P_{\min}$ penalizes the three phases in the decreasing order $FF > I_/ > EE$, as best illustrated in Fig. 6b. In contrast, the steric repulsion term F^P_{pol} decays either similarly with distance (for *FF* and $I_/$ phases) or remains constant (*EE* phase), and thus the increase in $d^P_{\min}$ does not reward the three phases as differently (in terms of decreasing steric repulsion). Thus, the *FF* phase, which is penalized the most in *overall* free energy, transitions to the least-penalized *EE* phase *via* the $I_/$ phase with intermediate penalty upon increasing σ_{pol} and/or decreasing ε_{cc}.

Second, the phase boundaries exhibit a parabolic dependence of ε_{cc} on σ_{pol}. In other words, phase transitions, such as those between the *FF* and $I_/$ phases or between $I_/$ and *EE* phases, becomes more sensitive to changes in σ_{pol} and less sensitive to changes in ε_{cc} with increasing magnitude of σ_{pol}. This is easily explained by the functional forms of the vdW and steric interaction energy terms. Whereas F^P_{cc} depends linearly on ε_{cc}, F^P_{pol} exhibits a cubic power-law dependence on σ_{pol}. Hence, the overall free energy, and thereby the phase transitions, are more sensitive to changes in σ_{pol} as compared to ε_{cc}.

Third, the $I_\parallel$ phase is observed only in a small sector of the parameter space in between the *FF* and *EE* phases at low σ_{pol} and ε_{cc} for all Γ and D. This is primarily because F^P_{cc} and F^P_{pol} expressions for both the $I_\parallel$ and *FF* phases scale similarly with respect to d_s, and differ from each other only in the relative magnitudes of the prefactors c and n_{conf}. Consequently, the phase boundary $\varepsilon_{cc}(\sigma_{pol})$ between these two phases exhibits a much gentler curvature compared to those between the other phases. The $I_\parallel$ phase is favored over the *FF* phase only at sufficiently large σ_{pol} and small ε_{cc} (Fig. S4a). In this region of the parameter space, the loss in vdW interactions associated with nanocube surfaces (in the *FF* phase) sliding off each other to form the $I_\parallel$ phase is more than compensated by the reduction in the steric repulsion associated with sliding. However, in a large portion of this region, the nanocubes

also prefer to form the *EE* phase over the $I_{\parallel}$ phase (Fig. S4b). This allows the nanocubes to fully eliminate all steric repulsion without sacrificing much vdW interactions given the large σ_{pol} associated with this region (in some cases the nanocubes may even exhibit stronger vdW interactions in the *EE* phase due to its contacting surfaces). As a result, the $I_{\parallel}$ phase appears as the globally stable phase in only a small window of the parameter space (Fig. S4c).

Fourth, the phase diagram shows that the $I_{/}$ phase broadened and encroached into both the *FF* and *EE* phases as Γ was increased (Figs. 10a-c). The encroachment into the $I_{/}$ phase may be explained by considering that the number of confined chains n_{conf} increases more dramatically with increasing Γ for the *FF* phase as compared to the $I_{/}$ phase. Specifically, the ratio of n_{conf} for the two phases is given by

$$\frac{n_{\text{conf}}^{FF}}{n_{\text{conf}}^{I_{/}}} = \sqrt{\Gamma} D. \tag{16}$$

Thus, an increase in Γ is more unfavorable, in terms of steric interactions, for the *FF* phase than $I_{/}$. The encroachment into the *EE* may also be explained in terms of increasing n_{conf}. While this increase amplifies the steric repulsion in the $I_{/}$ phase, as explained above, it also leads to reduced overlap between the nanocubes in the *EE* phase (via Eq. 11), which leads to a reduction in the vdW attraction. Apparently, the loss in vdW interactions for the *EE* phase is larger in magnitude than the increase in steric repulsion of the $I_{/}$ phase, causing the $I_{/}$ phase to also encroach into the *EE* phase.

Lastly, we observed the complete disappearance of the $I_{/}$ when D was increased from 10σ to 20σ (*cf.* Figs. 10a and d). This effect occurs because the vdW attraction F_{cc}^{P} scales linearly with D for the $I_{/}$ phase due to the tilted faces, whereas it exhibits a quadratic scaling with D for all remaining phases with parallel faces. Thus, the doubling of the nanocube size doubled the vdW attraction between nanocubes for the $I_{/}$ phase, but quadrupled the vdW attraction in the remaining phases, causing these phases to become more stable than the $I_{/}$ phase and leading to its disappearance from the phase diagram.

The scaling relationships also importantly allowed us to investigate phase behavior at much higher grafting densities than those explored by simulations, which focused on $\Gamma \leqslant 0.16/\sigma^2$. The derived relationships should remain valid for higher values of Γ as long as the grafted chains are in the mushroom regime. Larger grafting densities, however, yield an increasingly larger number of intermediate states $I_{/,n}$ and $I_{\parallel,n}$ exhibiting different extents of overlap between the two nanocubes. For convenience, we considered only one of these $I_{/}$ phases, where the edge of one nanocube contacted the face of the other nanocube at its middle (see Fig. S1d for details on estimating coefficients c for large Γ values), and ignored the $I_{\parallel}$ phase, which occupies only a small fraction of the parameter space.

Figure 11 shows various Γ–$\varepsilon_{\mathrm{cc}}$ cross-sections of the phase diagram obtained at three different values of σ_{pol} for the 10σ nanocubes. The scaling relations recapitulate the orientational phase behavior obtained from simulations with small Γ, even though the simulations considered all possible $I_{/,n}$ and $I_{\parallel,n}$ phases. More importantly, the scaling relations demonstrate that nanocubes exhibit very different phase behavior in the Γ–$\varepsilon_{\mathrm{cc}}$ parameter space depending on the magnitude of σ_{pol}. At $\sigma_{\mathrm{pol}} = 0.25\sigma$, the *FF* phase occupies a large portion of the phase diagram; in this regime, the nanocube faces are able to access small separation distances with strong vdW attraction, due to the small excluded volume of the polymer segments. Only at sufficiently high values of Γ, or sufficiently small values of $\varepsilon_{\mathrm{cc}}$, do the nanocube faces tilt to form the $I_{/}$ phase, as reflected in the small slope of *FF*–$I_{/}$ phase boundary. The *EE* phase forms only at very small values of $\varepsilon_{\mathrm{cc}}$, irrespective of the grafting density. When σ_{pol} increases to 0.5σ, the *FF*–$I_{/}$ phase boundary exhibits a sharper slope as the free energy of the *FF* phase is more adversely affected than the $I_{/}$ phase with decreasing $\varepsilon_{\mathrm{cc}}$ or increasing Γ, as discussed before. The *EE* phase, which is least affected by decreasing $\varepsilon_{\mathrm{cc}}$ (as the separation distance d_{s} remains constant in the *EE* phase while that of the other phases needs to expand in response to increasing *relative* strength of steric repulsion), then occupies a larger fraction of the phase diagram. At even larger values of $\sigma_{\mathrm{pol}} = 0.75\sigma$, the *FF* phase, interestingly, completely vanishes. In this regime, the large excluded volume of

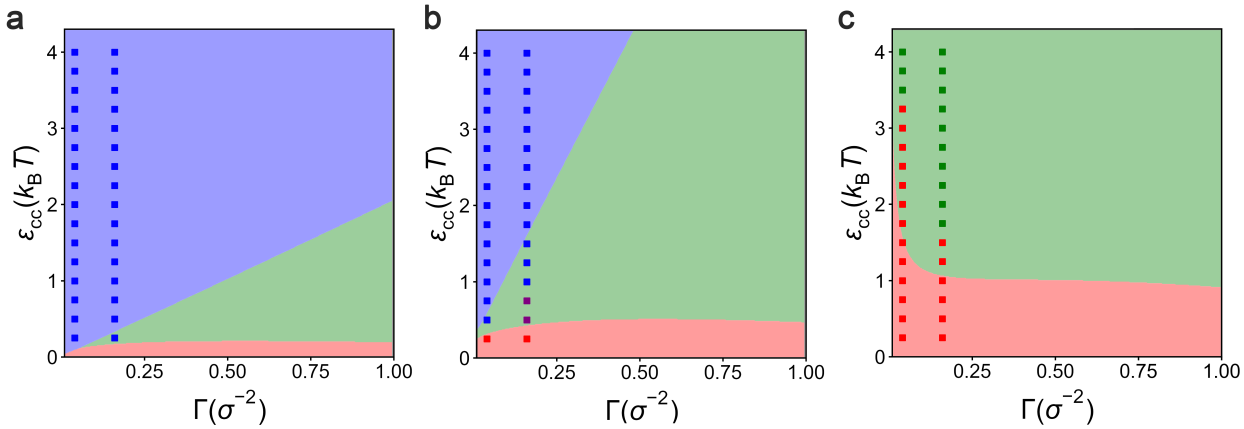

Figure 11: Phase diagram cross-sections in Γ–ε_{cc} obtained from scaling relations exploring a broader range of grafting densities for $D = 10\sigma$ nanocubes with: (a) $\sigma_{pol} = 0.25\sigma$, (b) $\sigma_{pol} = 0.5\sigma$, and (c) $\sigma_{pol} = 0.75\sigma$.

the graft segments pushes the nanocubes so far apart that they are no longer able to access strong vdW interactions (due to its sharp decay with distance), and the phase diagram is reduced to a competition between the $I_/$ and *EE* phases.

Discussion

One of the main results of this work is that grafted nanocubes exhibit a variety of thermodynamically stable interparticle configurations, which we classified into the *FF*, *EE*, $I_\parallel$, and $I_/$ phases based on the orientation and degree of overlap between the interacting faces of the nanocubes. This finding goes beyond our earlier investigation which considered only the *FF* and *EE* configurations. Our present work shows that the $I_\parallel$ and $I_/$ configurations are legitimate phases that occupy a large portion of the phase diagram, especially the $I_/$ phase that provides a compromise between the *FF* phase with strong interactions (both vdW attraction and steric repulsion) and the *EE* phase with weak interactions. In addition, our earlier study examined only the "idealized" *EE* configuration with touching edges, whereas we show here that the *EE* phase exhibits some overlap between the bare edges of the nanocube faces. The overlap allows for much stronger vdW interactions between the nanocubes without gaining much steric repulsion. For example, our current study predicts that $F_{cc}^{EE} = -301.2\varepsilon_{cc}$ for the

10σ nanocubes with $\Gamma = 0.16/\sigma^2$, whereas $F_{cc} = -85.1\varepsilon_{cc}$ in the idealized *EE* configuration. The amount of overlap was found to decrease with increasing grafting density, implying that the idealized *EE* configuration would occur only when the grafted chains covered the entire face of the nanocubes. While this may be the case at high grafting densities, dense grafting and uniform coverage of the surfaces are not always possible, especially near the edges of the nanocubes.

Our finding of the partly overlapped *EE* phase and the $I_{\parallel}$, and $I_{/}$ phases also provides a possible explanation for the various kinds of "imperfect" nanocube configurations obtained experimentally.[16,17,39,40] For instance, assembly experiments on polyethylene glycol (PEG)-grafted Ag nanocubes observed face-edge configurations with a wide range of angles between the contacting surfaces similar to our $I_{/}$ phase, and configurations with partly overlapping parallel faces similar to our *EE* and $I_{\parallel}$ phases (see, for example, Fig. 5 of Gurunatha et al.[17]). While these configurations were initially attributed to grafting imperfections or to kinetically trapped states, our results demonstrate that these observed configurations could also represent thermodynamically stable states.

Another key result of this work is the orientational phase diagram we obtained, which should provide guidance to researchers for predicting orientational phases based on nanocube parameters or, *vice versa*, designing nanocubes to achieve specific phases. The phase diagram cross-sections plotted in Fig. 10 indicate that increasingly larger changes in the vdW interaction strength ε_{cc} or polymer segment excluded volume σ_{pol} are required to observe phase transitions between the *FF*, $I_{/}$, and *EE* phases when the nanocubes exhibit strong vdW and/or steric interactions. For instance, nanocubes with $\varepsilon_{cc} = 3\ k_B T$ and $\sigma_{pol} = 0.75\sigma$ exhibiting the $I_{/}$ phase in Fig. 10b would require about a $2k_B T$ reduction in ε_{cc} or a 0.25σ increase in σ_{pol} to convert nanocube configurations into the *EE* phase. Thus, strong vdW and steric interactions between nanocubes are required to achieve highly stable orientational phases. Contrarily, the opposite strategy of designing nanocubes with weak interactions could be used for assembling weakly stable phases. For example, nanocubes exhibit a "triple

point" at low ε_{cc} and σ_{pol} where all three phases *FF*, $I_{\|}$, and $I_{/}$ coexist (see Fig. 10). Nanocube orientations near the triple point are expected to be very sensitive to small changes in ε_{cc} and σ_{pol} that could for instance be brought about by changing external conditions (e.g., temperature and pH). This concept raises the intriguing possibility of creating reconfigurable phases that can reversibly switch between distinct orientational states based on small external field triggers. Lastly, Fig. 11 demonstrates that altering the grafting density Γ is not a viable approach for achieving the *EE* phase. While an increase in Γ leads to suppression of the *FF* state, the nanocubes transition to the $I_{/}$ phase rather than the *EE* states. Thus, changes in parameter like ε_{cc} or σ_{pol} are recommended over changes in Γ to induce the *EE* configuration.

The trends from the computed phase diagram agree well with the limited amount of experimental work carried out so far on polymer-grafted nanocubes. For example, one set of experiments have shown that large nanocubes ($D = 45$ nm) assemble into *FF* configurations with much higher propensities than smaller nanocubes ($D = 25$ nm).[39] While this may not seem obvious, as larger nanocubes also carry more grafted chains, comparison of phase diagram cross-sections at two different nanocube sizes (see Fig. 10a and d) shows that the *FF* phase indeed becomes more dominant with increasing size. Another set of experiments have found that nanocubes transition from face-face to face-edge to edge-edge configurations with an increase in the molecular weights of the grafted chains.[17] This sequence of transitions in interparticle orientation mirrors the phase transitions observed in our phase diagram with increasing steric repulsion from grafted chains (see Fig. 10). This encouraging congruence with experiments illustrate the value of our computational predictions in guiding experiments on polymer-grafted nanocube systems.

A third important result is the analytical expressions for the free energies of the orientational phases developed in this study. These expressions allowed us to construct a more comprehensive phase diagram than afforded by simulations alone, and also provided simple, physically intuitive explanations for the various features exhibited by the phase diagram. For instance, the expansion and contraction of the $I_{/}$ phase region with increasing grafting

density and nanocube size, respectively, could be easily explained through differences in the free energy scalings of $I_{/}$ phase as compared to those of the *FF* and *EE* phases; These scaling differences in turn arose from the slanted configuration of the interacting nanocubes in the $I_{/}$ phase *versus* the parallel configuration exhibited by the remaining phases. Moreover, the free energies are provided as simple functions of experimentally accessible parameters that could be readily used by researchers to study the phase behavior of other kinds of faceted, polymer-grafted nanoparticles, as long as the underlying assumptions of the model are not violated.

All these results discussed above would be especially relevant for plasmonic applications. Studies have shown that plasmonic resonances exhibited by clusters and larger assemblies of faceted NPs made out of plasmonically-active metals like Ag or Au are sensitive to not only the size of the gap between NPs, but also their relative orientations.[16,39,41,42] Differences in the surface curvatures of particle faces and edges lead to distinct electromagnetic field localization effects. In the case of nanocubes, field localization is concentrated at the edge-edge junction in *EE* configurations, while the field is delocalized over the entire face-face junction in *FF* configurations. In one study, these effects led *EE*-oriented chains of nanocubes to exhibit red-shifted surface plasmons (compared to isolated nanocubes) and *FF* chains to exhibit broadband scattering.[16] Such plasmonic couplings also lead to huge enhancements in electric fields and Raman spectra in closely-spaced assemblies of nanocubes compared to assemblies of spherical NPs or nanocubes present in a dispersed state.[39] These studies clearly demonstrate the need to understand interparticle interactions and to control their spacings and orientations.

Our results come with several caveats. First, all nanocube phases involving confined grafts exhibited *equilibrium* surface separation distances smaller than the Kuhn length of the grafts. This effect stems from the strong, short-ranged nature of vdW interactions between nanocubes and the mushroom-like conformations of the grafted chains, where the enthalpic advantage gained from decreasing the separation distance outweighs the entropic

penalty of squeezing the grafts. Only at separation distance smaller than the Kuhn length does the repulsion become comparable to the vdW attraction. At this point, the behavior of the grafts is more akin to that of confined particles than polymer chains, as noted from the LJ-like behavior of the steric repulsion term (Eq. 13). For the nanocube sizes investigated in this study, this is true even when the grafted chains are much longer as the polymer segments can escape out of the junction between the nanocubes (Fig. S5). However, we expect that significantly stiffer grafts or longer grafts on larger nanocubes would lead to much larger entropic penalties of confinement, and thereby equilibrium separation distances larger than the Kuhn length. In this regime, the steric repulsion may scale differently with distance.[43] Thus, the phase diagram presented in this study may no longer be numerically accurate in this regime, though its overall features should likely be preserved. This study also did not investigate systems in which nanocubes assemble due to attractive polymer-polymer interactions. While the LJ potential used for modeling polymer-nanocube interactions has both attractive and repulsive portions, the small separation distances mandated that all of polymer-cube interactions were in the repulsive region. Therefore, the grafts only provided steric repulsion and never acted as "bridging agents" between the nanocubes. Previous studies have demonstrated that attractive polymer-nanocube interactions could also play a role in determining their orientations.[16,17] Further studies with longer/stiffer grafts and stronger polymer-nanocube interactions are required to properly reveal the role of these effects on nanocube phase behavior.

Another effect neglected in this study is the depletion force arising from the solvent, which can be quite large in polymeric melts.[32] Depletion effects may be even more important for nanocubes, which provide a larger surface area of interaction compared to spherical particles, and hence larger overlaps between their solvent-excluded volumes. For instance, rod-like particles were found to be more significantly affected by depletion effects than spherical particles.[44] We hypothesize that the FF and $I_{\parallel}$ phases with larger overlap between their solvent-excluded volumes will exhibit larger depletion interactions and will be favored over

the $I_{/}$ and EE phases. Future studies with explicitly-modeled solvents should reveal the magnitude of such orientation-dependent depletion effects and the extent to which they affect the phase behavior of nanocubes.

It should also be noted that our results were obtained using idealized systems. Experimental systems are however likely to exhibit uneven surface grafting of polymer chains, polydispersity in the length of the polymer grafts, and variations in the size and shape of the nanocubes, including rounding of their edges and corners, each of which could affect particle assembly in distinct ways. For example, in this work we considered uniform spatial distribution of grafts on nanocube faces. This may be a reasonable approximation for short grafts chemically attached as fully-grown chains from the solution onto the surface of the NPs via a "grafting-to" mechanism,[16] whereby chains tend to attach more or less uniformly to surfaces.[45] Hence, one would expect such chains to predominanly attach to nanocube faces due to the much larger surface area they present for attachment as compared edges. However, longer and densely-grafted polymers have been shown to preferentially graft to the edges of the nanocubes where they are less sterically constrained by other chains.[46] Therefore, the scaling relationships and the phase diagram presented here should be treated as general guiding principles rather than quantitative solutions for controlling the orientations of nanocubes in their assemblies.

Lastly, our current work focused on the orientational behavior of an *isolated* pair of polymer-grafted nanocubes. We did not account for steric constraints and other multi-body interactions that may also influence interparticle orientations in larger assemblies of nanocubes. Nevertheless, the results obtained here should still be applicable to assembly of grafted nanocubes at low particle volume fraction, where nanocubes tend to assemble into quasi-linear chains.[16,17,39] Indeed, most of the experimental results used earlier to demonstrate agreement between experiments and computational predictions were taken from such linear assemblies. Interestingly, our results also seem to relate well to crystal lattices of nanocubes grafted with single-stranded DNA or organic ligands that were assembled via

DNA hybridization or solvent evaporation, respectively.[46,47] These studies showed a transition from simple cubic (SC) to body-centered tetragonal (BCT) lattices with increasing steric repulsion between grafts brought about by increasing the length of the DNA strands or swelling the ligand grafts. In effect, nanocubes exhibiting face-face contacts in the SC lattice translated and rotated into a BCT lattice with partly-overlapping nanocube faces to minimize the steric repulsion from their grafts, very similar to the $FF \rightarrow I_{\parallel}$ phase transition observed in our simulations. Thus, unlike polymer-grafted spherical NPs which have access to only translational degrees of freedom to minimize their interaction free energy, structures assembled from polymer-grafted nanocubes must take into account both translational and rotational degrees of freedom.

Conclusions

We investigated the orientational phase behavior of polymer-grafted nanocubes using MC simulations and free-energy scaling relations derived from simulations. Consistent with experiments, our simulations predicted that the nanocubes may assemble into face-face, edge-edge, or a spectrum of intermediate configurations of varying overlap with parallel or slanted faces. The simulation results also helped us in formulating simple analytical expressions for the free energies of these four phases. The free energies were found to exhibit distinct scalings with respect to nanocube size, separation distance, and grafting densities for the four phases as a result of their geometric differences. The free energies were also used to construct an orientational phase diagram over a multi-dimensional parameter space comprised of nanocube size, nanocube interaction strength, grafting density, and polymer segment size. We showed how the morphology of the phase diagram is intrinsically related to differences in the free energy scalings of the four phases. Overall, these results demonstrate how particle size, interactions, and polymer grafting could be used to control the relative orientation and overlap between adjacent nanoparticles in their higher-order assemblies. Ultimately, such control

should enable fabrication of advanced catalytic, optical, and plasmonic nanocomposites with precisely-oriented nanoparticles with their assemblies.

Acknowledgement

We thank National Science Foundation (CMMI Award 1636356) for partial support of this research. Computational resources were provided by the Extreme Science and Engineering Discovery Environment (XSEDE) Program supported by the National Science Foundation (ACI-1053575) and the Duke Compute Cluster.

Supporting Information Available

Effect of nanocube size on the free energies of vdW and polymer-nanocube interactions. Distance normalization of the polymer-cube interaction free energy. Surface roughness effect on polymer-nanocube potential energies. Intermediate phase diagrams for subsets of available phases. Dependence of number of polymer segments confined between interacting surfaces on polymer chain length.

References

(1) Glotzer, S. C.; Solomon, M. J. Anisotropy of building blocks and their assembly into complex structures. *Nat. Mater.* **2007**, *6*, 557.

(2) Crassous, J. J.; Mihut, A. M.; Wernersson, E.; Pfleiderer, P.; Vermant, J.; Linse, P.; Schurtenberger, P. Field-induced assembly of colloidal ellipsoids into well-defined microtubules. *Nat. Commun.* **2014**, *5*, 5516.

(3) Keville, K.; Franses, E.; Caruthers, J. Preparation and characterization of monodisperse polymer microspheroids. *J. Colloid Interface Sci.* **1991**, *144*, 103–126.

(4) Lee, A.; Andrade, G. F. S.; Ahmed, A.; Souza, M. L.; Coombs, N.; Tumarkin, E.; Liu, K.; Gordon, R.; Brolo, A. G.; Kumacheva, E. Probing Dynamic Generation of Hot-Spots in Self-Assembled Chains of Gold Nanorods by Surface-Enhanced Raman Scattering. *J. Am. Chem. Soc.* **2011**, *133*, 7563–7570.

(5) Plascencia-Villa, G.; Bahena, D.; Rodriguez, A. R.; Ponce, A.; Jose-Yacaman, M. Advanced microscopy of star-shaped gold nanoparticles and their adsorption-uptake by macrophages. *Metallomics* **2013**, *5*, 242–250.

(6) Kim, S.; Jin, J.; Kim, Y.-J.; Park, I.-Y.; Kim, Y.; Kim, S.-W. High-harmonic generation by resonant plasmon field enhancement. *Nature* **2008**, *453*, 757.

(7) Sun, Y.; Xia, Y. Shape-controlled synthesis of gold and silver nanoparticles. *Science* **2002**, *298*, 2176–2179.

(8) Wang, Y.; Wang, Y.; Breed, D. R.; Manoharan, V. N.; Feng, L.; Hollingsworth, A. D.; Weck, M.; Pine, D. J. Colloids with valence and specific directional bonding. *Nature* **2012**, *491*, 51.

(9) Love, J. C.; Gates, B. D.; Wolfe, D. B.; Paul, K. E.; Whitesides, G. M. Fabrication and wetting properties of metallic half-shells with submicron diameters. *Nano Lett.* **2002**, *2*, 891–894.

(10) Greyson, E. C.; Barton, J. E.; Odom, T. W. Tetrahedral Zinc Blende Tin Sulfide Nano- and Microcrystals. *Small* **2006**, *2*, 368–371.

(11) Love, J. C.; Gates, B. D.; Wolfe, D. B.; Paul, K. E.; Whitesides, G. M. Fabrication and wetting properties of metallic half-shells with submicron diameters. *Nano Lett.* **2002**, *2*, 891–894.

(12) Chen, S.; Wang, Z. L.; Ballato, J.; Foulger, S. H.; Carroll, D. L. Monopod, bipod, tripod, and tetrapod gold nanocrystals. *J. Am. Chem. Soc.* **2003**, *125*, 16186–16187.

(13) Lee, S.-M.; Jun, Y.-w.; Cho, S.-N.; Cheon, J. Single-crystalline star-shaped nanocrystals and their evolution: programming the geometry of nano-building blocks. *J. Am. Chem. Soc.* **2002**, *124*, 11244–11245.

(14) Tang, Z.; Wang, Y.; Shanbhag, S.; Giersig, M.; Kotov, N. A. Spontaneous transformation of CdTe nanoparticles into angled Te nanocrystals: from particles and rods to checkmarks, X-marks, and other unusual shapes. *J. Am. Chem. Soc.* **2006**, *128*, 6730–6736.

(15) Gao, B.; Alvi, Y.; Rosen, D.; Lav, M.; Tao, A. R. Designer nanojunctions: orienting shaped nanoparticles within polymer thin-film nanocomposites. *Chem. Commun.* **2013**, *49*, 4382–4384.

(16) Gao, B.; Arya, G.; Tao, A. R. Self-orienting nanocubes for the assembly of plasmonic nanojunctions. *Nat. Nanotechnol.* **2012**, *7*, 433–437.

(17) Gurunatha, K. L.; Marvi, S.; Arya, G.; Tao, A. R. Computationally Guided Assembly of Oriented Nanocubes by Modulating Grafted Polymer–Surface Interactions. *Nano Lett.* **2015**, *15*, 7377–7382.

(18) Hsiao, L. C.; Schultz, B. A.; Glaser, J.; Engel, M.; Szakasits, M. E.; Glotzer, S. C.; Solomon, M. J. Metastable orientational order of colloidal discoids. *Nat. Commun.* **2015**, *6*, 8507.

(19) Green, E.; Fullwood, E.; Selden, J.; Zharov, I. Functional membranes via nanoparticle self-assembly. *Chem. Commun.* **2015**, *51*, 7770–7780.

(20) Bilchak, C. R.; Buenning, E.; Asai, M.; Zhang, K.; Durning, C. J.; Kumar, S. K.; Huang, Y.; Benicewicz, B. C.; Gidley, D. W.; Cheng, S.; Sokolov, A. P.; Minelli, M.; Doghieri, F. Polymer-grafted nanoparticle membranes with controllable free volume. *Macromolecules* **2017**, *50*, 7111–7120.

(21) Zheng, J.; Li, X.; Gu, R.; Lu, T. Comparison of the surface properties of the assembled silver nanoparticle electrode and roughened silver electrode. *J. Phys. Chem. B* **2002**, *106*, 1019–1023.

(22) Young, S. L.; Kellon, J. E.; Hutchison, J. E. Small gold nanoparticles interfaced to electrodes through molecular linkers: a platform to enhance electron transfer and increase electrochemically active surface area. *J. Am. Chem. Soc.* **2016**, *138*, 13975–13984.

(23) Hsu, S.-W.; Rodarte, A. L.; Som, M.; Arya, G.; Tao, A. R. Colloidal Plasmonic Nanocomposites: From Fabrication to Optical Function. *Chem. Rev.* **2018**, *118*, 3100–3120.

(24) Nie, Z.; Fava, D.; Rubinstein, M.; Kumacheva, E. "Supramolecular" assembly of gold nanorods end-terminated with polymer "pom-poms": effect of pom-pom structure on the association modes. *J. Am. Chem. Soc.* **2008**, *130*, 3683–3689.

(25) Meng, D.; Kumar, S. K.; Lane, J. M. D.; Grest, G. S. Effective interactions between grafted nanoparticles in a polymer matrix. *Soft Matter* **2012**, *8*, 5002–5010.

(26) Hattemer, G. D.; Arya, G. Viscoelastic properties of polymer-grafted nanoparticle composites from molecular dynamics simulations. *Macromolecules* **2015**, *48*, 1240–1255.

(27) Akcora, P.; Liu, H.; Kumar, S. K.; Moll, J.; Li, Y.; Benicewicz, B. C.; Schadler, L. S.; Acehan, D.; Panagiotopoulos, A. Z.; Pryamitsyn, V.; Ganesan, V.; Ilavsky, J.; Thiyagarajan, P.; Colby, R. H.; Douglas, J. F. Anisotropic self-assembly of spherical polymer-grafted nanoparticles. *Nat. Mater.* **2009**, *8*, 354.

(28) Lafitte, T.; Kumar, S. K.; Panagiotopoulos, A. Z. Self-assembly of polymer-grafted nanoparticles in thin films. *Soft Matter* **2014**, *10*, 786–794.

(29) Phillips, C. L.; Glotzer, S. C. Effect of nanoparticle polydispersity on the self-assembly of polymer tethered nanospheres. *J. Chem. Phys.* **2012**, *137*, 104901.

(30) Chan, E. R.; Zhang, X.; Lee, C.-Y.; Neurock, M.; Glotzer, S. C. Simulations of Tetra-Tethered Organic/Inorganic Nanocube-Polymer Assemblies. *Macromolecules* **2005**, *38*, 6168–6180.

(31) Lin, Y.-L.; Chiou, C.-S.; Kumar, S. K.; Lin, J.-J.; Sheng, Y.-J.; Tsao, H.-K. Self-assembled superstructures of polymer-grafted nanoparticles: effects of particle shape and matrix polymer. *J. Phys. Chem. C* **2011**, *115*, 5566–5577.

(32) Tang, T.-Y.; Arya, G. Anisotropic Three-Particle Interactions between Spherical Polymer-Grafted Nanoparticles in a Polymer Matrix. *Macromolecules* **2017**, *50*, 1167–1183.

(33) Jorgensen, W. L.; Maxwell, D. S.; Tirado-Rives, J. Development and Testing of the OPLS All-Atom Force Field on Conformational Energetics and Properties of Organic Liquids. *J. Am. Chem. Soc.* **1996**, *118*, 11225–11236.

(34) Rowlinson, J. S.; Swinton, F. L. *Liquids and liquid mixtures*; Butterworth-Heinemann, 1982.

(35) Siepmann, J. I.; Frenkel, D. Configurational bias Monte Carlo: a new sampling scheme for flexible chains. *Mol. Phys.* **1992**, *75*, 59–70.

(36) Arya, G. Energetic and Entropic Forces Governing the Attraction between Polyelectrolyte-Grafted Colloids. *J. Phys. Chem. B* **2009**, *113*, 15760–15770.

(37) Rojas, O. J.; Lokanathan, A. R.; Kontturi, E.; Laine, J.; Bock, H. The unusual interactions between polymer grafted cellulose nanocrystal aggregates. *Soft Matter* **2013**, *9*, 8965–8973.

(38) Israelachvili, J. N. *Intermolecular and surface forces*; Academic press, 2011.

(39) Klinkova, A.; Thérien-Aubin, H.; Ahmed, A.; Nykypanchuk, D.; Choueiri, R. M.; Gagnon, B.; Muntyanu, A.; Gang, O.; Walker, G. C.; Kumacheva, E. Structural and

Optical Properties of Self-Assembled Chains of Plasmonic Nanocubes. *Nano Lett.* **2014**, *14*, 6314–6321.

(40) Gao, B.; Alvi, Y.; Rosen, D.; Lav, M.; R. Tao, A. Designer nanojunctions: orienting shaped nanoparticles within polymer thin-film nanocomposites. *Chem. Commun.* **2013**, *49*, 4382–4384.

(41) Lee, S. Y.; Hung, L.; Lang, G. S.; Cornett, J. E.; Mayergoyz, I. D.; Rabin, O. Dispersion in the SERS Enhancement with Silver Nanocube Dimers. *ACS Nano* **2010**, *4*, 5763–5772.

(42) Hooshmand, N.; Mousavi, H. S.; Panikkanvalappil, S. R.; Adibi, A.; El-Sayed, M. A. High-sensitivity molecular sensing using plasmonic nanocube chains in classical and quantum coupling regimes. *Nano Today* **2017**, *17*, 14–22.

(43) Chen, J. Z. Y.; Sullivan, D. E. Free Energy of a Wormlike Polymer Chain Confined in a Slit: Crossover between Two Scaling Regimes. *Macromolecules* **2006**, *39*, 7769–7773.

(44) Zanella, M.; Bertoni, G.; Franchini, I. R.; Brescia, R.; Baranov, D.; Manna, L. Assembly of shape-controlled nanocrystals by depletion attraction. *Chem. Commun.* **2011**, *47*, 203–205.

(45) Asai, M.; Zhao, D.; Kumar, S. K. Role of Grafting Mechanism on the Polymer Coverage and Self-Assembly of Hairy Nanoparticles. *ACS Nano* **2017**, *11*, 7028–7035.

(46) Lu, F.; Vo, T.; Zhang, Y.; Frenkel, A.; Yager, K. G.; Kumar, S.; Gang, O. Unusual packing of soft-shelled nanocubes. *Sci. Adv.* **2019**, *5*, eaaw2399.

(47) Quan, Z.; Xu, H.; Wang, C.; Wen, X.; Wang, Y.; Zhu, J.; Li, R.; Sheehan, C. J.; Wang, Z.; Smilgies, D.-M.; Luo, Z.; Fang, J. Solvent-Mediated Self-Assembly of Nanocube Superlattices. *J. Am. Chem. Soc.* **2014**, *136*, 1352–1359.

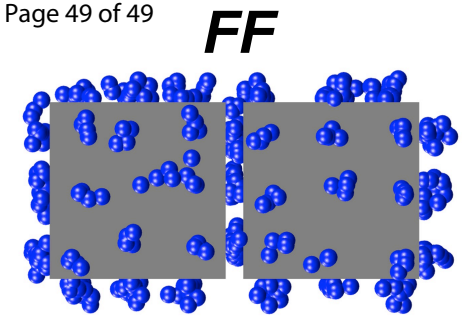
FF

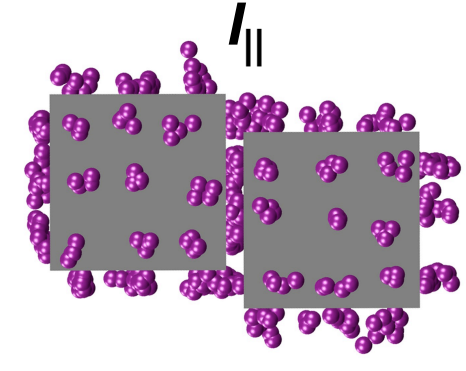
$I_{||}$

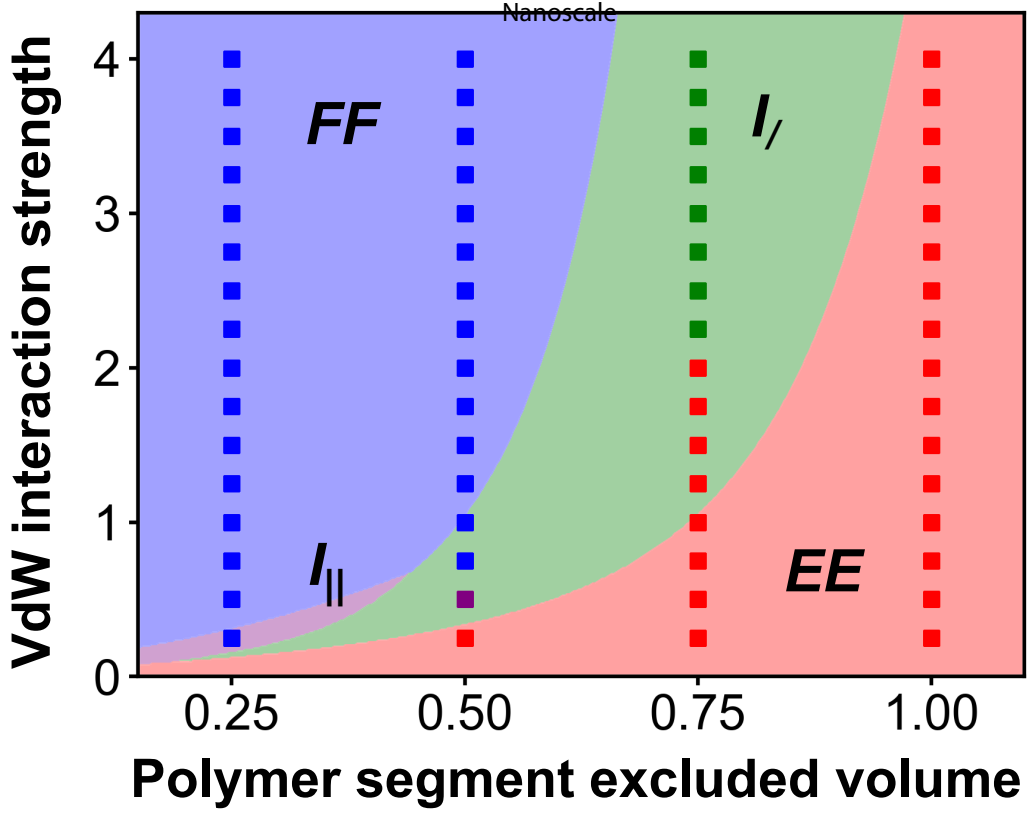
VdW interaction strength
0
1
2
3
4
0.25
0.50
0.75
1.00
Polymer segment excluded volume
FF
$I_{||}$
$I_{/}$
EE

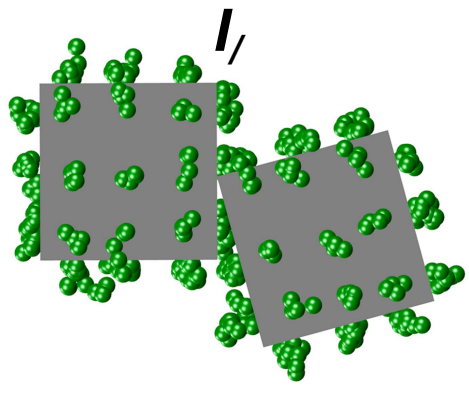
$I_{/}$

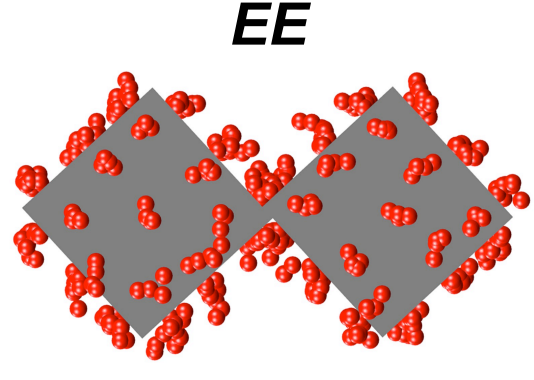
EE